N-6-methyladenosine (m6A) Promotes the Nuclear Retention of mRNAs with Intact 5′ Splice Site Motifs

Eliza S. Lee[1,6], Harrison. W. Smith[1], Yifan E. Wang[1], Sean S. J. Ihn[1], Leticia Scalize de Olivera[1], Nevraj S. Kejiou[1], Yijing L. Liang[2], Syed Nabeel-Shah[3,4], Robert Y. Jomphe[1,5], Shuye Pu[4], Jack F. Greenblatt[3,4], Alexander F. Palazzo[1,7]

1- University of Toronto, Department of Biochemistry, Canada

2- Centre for Computational Medicine, Hospital for Sick Children, Toronto, Canada

3- University of Toronto, Department of Molecular Genetics, Canada

4- Terrence Donnelly Centre for Cellular & Biomolecular Research, Toronto, Canada

5- Cell Biology Program, Hospital for Sick Children, Toronto, Canada

6- Present Address: Department of Biochemistry, University of Colorado Boulder, CO

7- Corresponding author

22

Abstract

In humans, misprocessed mRNAs containing intact 5′ Splice Site (5′SS) motifs are nuclear retained and targeted for decay by ZFC3H1, a component of the Poly(A) Exosome Targeting complex, and U1-70K, a component of the U1 snRNP. In *S. pombe*, the ZFC3H1 homolog, Red1, binds to the YTH-domain containing protein Mmi1 to target certain RNA transcripts to nuclear foci for nuclear retention and decay. Here we show that YTHDC1 and YTHDC2, two YTH domain-containing proteins that bind to *N*-6-methyladenosine (m6A) modified RNAs, interact with ZFC3H1 and U1-70K, and are required for the nuclear retention of mRNAs with intact 5′SS motifs. Disruption of m6A deposition inhibits both the nuclear retention of these transcripts and their accumulation in YTHDC1-enriched foci that are adjacent to nuclear speckles. Endogenous RNAs with intact 5′SS motifs, such as intronic polyadenylated transcripts, tend to be m6A-modified at low levels. Thus, m6A modification acts in a conserved quality control mechanism that targets misprocessed mRNAs for nuclear retention and decay.

Introduction

Eukaryotic cells are divided into two compartments: the nucleus where pre-mRNAs are synthesized and processed, and the cytoplasm where mature mRNAs are translated into proteins. This subcellular division allows for extensive quality control at the level of both RNA synthesis and RNA processing to promote the nuclear retention and degradation of spurious transcripts and misprocessed mRNAs before they access the translation machinery in the cytoplasm (Palazzo and Lee 2018; Garland and Jensen 2020; Palazzo et al. 2024). Misprocessed mRNAs typically contain intact RNA processing *cis*-elements which promote retention and decay (Legrain and Rosbash 1989; Abad et al. 2008; Lee et al. 2015).

One class of misprocessed mRNAs are intronic polyadenylated (IPA) transcripts (Tian et al. 2007). These are generated by cryptic 3′cleavage/polyadenylation signals found in introns. Although most of these cryptic 3′cleavage/polyadenylation signals are suppressed (Kaida et al. 2010), they can be used at low levels to generate IPA transcripts that tend to encode protein fragments (Ogami et al. 2017), which are often toxic as they can compete with endogenous proteins for their binding partners (Veitia 2007). IPA transcripts contain intact 5' splice site (5′SS) motifs, which are present at the boundary between the upstream exon and the intron where the 3′ cleavage occurs. We and others have shown that the presence of an intact 5′SS motif in an RNA promotes its nuclear retention and decay (Legrain and Rosbash 1989; Abad et al. 2008; Lee et al. 2015). These transcripts are recognized by the U1 snRNP, and the U1 component U1-70K is required for their nuclear retention and decay (Fortes et al. 2003; Abad et al. 2008; Goraczniak et al. 2009; Lee et al. 2022). We previously found that U1-70K associates with ZFC3H1 (Lee et al. 2022), a component of the Poly(A) Exosome Targeting (PAXT) complex. Moreover, we and others have shown that ZFC3H1 is required for the nuclear retention and decay of RNAs with

60 intact 5′SS motifs including IPA transcripts (Ogami et al. 2017; Lee et al. 2022). PAXT also
61 contains the nuclear poly(A) binding protein, PABPN1, and the RNA helicase MTR4, which is
62 known to feed RNAs into the nuclear exosome, the major RNase complex in human cells (Meola
63 et al. 2016; Ogami et al. 2017; Ogami and Manley 2017; Silla et al. 2018, 2020). Although
64 MTR4 is not required for nuclear retention, PABPN1 likely plays a role (Lee et al. 2022).

65 The PAXT complex is conserved between humans and *S. pombe*, where it is known as the
66 MTREC (Mtl1-Red1 Core) complex, and is composed of Mtl1, the paralogue of Mtr4, Red1, the
67 paralogue of ZFC3H1 and Pab2, a poly(A) binding protein (Sugiyama and Sugioka-Sugiyama
68 2011; Zhou et al. 2015; Shichino et al. 2020). MTREC promotes the nuclear retention and decay
69 of meiotic mRNAs that are inappropriately synthesized in interphase cells. MTREC is recruited
70 to these RNAs through a complex of three proteins consisting of Erh1, Pir1 and Mmi1
71 (Sugiyama and Sugioka-Sugiyama 2011; Sugiyama et al. 2016; Wei et al. 2021; Shichino et al.
72 2020). Note that Pir1 has a Serine/Proline-rich region that shows a limited homology with the N-
73 terminus of ZFC3H1 (Wei et al. 2021) and that Mmi1 contains a YTH domain, which in other
74 systems recognizes *N*-6-methyladenosine (m6A) modified RNAs. In *S. pombe*, no m6A
75 modification is detectable in mRNAs (Ishigami et al. 2021) and instead Mmi1 binds to specific
76 RNA motifs (Chen et al. 2011; Sugiyama and Sugioka-Sugiyama 2011; Wang et al. 2016).
77 MTREC and Mmi1 are also involved in the nuclear retention and decay of non-coding RNAs
78 (ncRNAs) and transposable element-derived RNAs (Sugiyama et al. 2016; Vo et al. 2019; Zhou
79 et al. 2015). When RNA decay is inhibited, MTREC-targeted RNAs accumulate in a
80 Mmi1/Red1-enriched nuclear foci (Sugiyama and Sugioka-Sugiyama 2011; Shichino et al. 2018,
81 2020).

82 In humans, YTH domains recognize m6A modified RNAs (Xu et al. 2014). This
83 modification is enriched in several regions of mRNAs, including large exons, regions
84 surrounding the stop codon, and 3′UTRs (Dominissini et al. 2012; Meyer et al. 2012), and is
85 depleted around exon-exon junctions (Yang et al. 2022; Uzonyi et al. 2023; He et al. 2023; Luo
86 et al. 2023). The m6A modification is catalyzed by the METTL3 methyltransferase, which forms
87 a complex with METTL14 and other factors (Liu et al. 2014). This modification can be removed
88 by the demethylases ALKBH5, FTO and perhaps ALKBH3 (Jia et al. 2011; Zheng et al. 2013;
89 Ueda et al. 2017). m6A is predominantly recognized by five YTH domain containing proteins in
90 humans, including YTHDC1 and YTHDC2, which are localized to the nucleoplasm (Xu et al.
91 2021).

92 Initial studies indicated that the m6A modification, and m6A-binding proteins promote
93 mRNA export (Roundtree et al. 2017; Zheng et al. 2013; Lesbirel et al. 2018; Lesbirel and
94 Wilson 2019); however, more recent work has found that the levels of m6A modification
95 correlate with nuclear retention (Tang et al. 2024). Moreover, m6A and YTHDC1 are required
96 for the suppression of RNAs generated from transposable elements, enhancer RNAs and other
97 ncRNAs (Liu et al. 2020), reminiscent of the function of MTREC and Mmi1 in *S. pombe*. Like
98 Mmi1 and Red1, YTHDC1 and ZFC3H1 are found in nuclear foci that contain mRNA (Cheng et
99 al. 2021; Nayler et al. 2000; Wang et al. 2021). These foci partially overlap nuclear speckles,
100 which are required for the nuclear retention of mRNA with intact 5′SS motifs (Lee et al. 2022).

101 Here we show that m6A modification is required for the efficient nuclear retention of
102 mRNAs that contain intact 5′SS motifs, which are found in IPA transcripts, and retains these in
103 nuclear foci present adjacent to nuclear speckles.

104

Results

YTHDC1 and YTHDC2 interact with both ZFC3H1 and U1-70K

In *S. pombe*, the MTREC associates with Mmi1, a nuclear YTH domain-containing protein (Figure 1A, left) (Sugiyama and Sugioka-Sugiyama 2011; Chen et al. 2011; Zhou et al. 2015; Shichino et al. 2020). To determine whether components of the equivalent human complex (known as PAXT, Figure 1A right) interact with nuclear YTH domain-containing proteins, we expressed either FLAG-HA-YTHDC1 or FLAG-ZFC3H1-HA in HEK293 cells and assessed their binding partners by co-immunoprecipitation in the absence or presence of RNase, which removed all detectable RNA from the lysate (Figure S1A). In FLAG-HA-YTHDC1 immunoprecipitates, we detected both endogenous ZFC3H1 and U1-70K, even in the presence of RNase (Figure 1B, S1B). FLAG-HA-YTHDC1 immunoprecipitates also contained YTHDC2 but not any detectable ALKBH5 (Figure 1B, S1B). In FLAG-ZFC3H1-HA immunoprecipitates, we detected endogenous YTHDC1, YTHDC2 and U1-70K, even in the presence of RNase, but not eIF4AIII or G3BP2 (Figure 1C-D, S1C). In all cases, the plasmid-expressed proteins were present at levels that were less than 10 fold the endogenous protein level and had only minor effects on the levels of their interacting partners (Figure S1D-J). When we immunoprecipitated a smaller fragment of FLAG-ZFC3H1 (FLAG-ZFC3H1 1-1233), which lacks the C-terminal TPR repeats but contains all known protein interaction-domains (Wang et al. 2021), we again detected YTHDC1, YTHDC2 and U170K in the precipitates, but not ALKBH5, eIF4AIII, METTL3 or ALY (Figure 1E-F).

These results indicate that nuclear YTH proteins associate with ZFC3H1 and U1-70K, two factors required for the nuclear retention of RNAs that contain intact 5′SS motifs.

128

129 **DRACH motifs are required for the efficient nuclear retention of mRNAs with an intact**
130 **5′SS motif**

131 The m6A methyltransferase METTL3 preferentially modifies RNAs at consensus
132 DRACH motifs (G/A/U, A/G, A, C, A/U/C) (Meyer et al. 2012; Dominissini et al. 2012). To test
133 whether m6A was required for nuclear retention, we mutated the DRACH motifs in the *fushi-*
134 *tarazu* (*ftz*) reporter which we previously used to study the effect of the 5′SS motif on nuclear
135 retention (Lee et al. 2015). For the parental intronless *ftz* reporter (*ftz-Δi*) we identified ten
136 putative DRACH motifs and for the 5′SS motif containing version (*ftz-Δi-5′SS*) we found eleven
137 motifs (Figure 2A). We mutated all but of one of the DRACH sites to generate two other
138 reporters, *no-m6A-ftz-Δi* and *no-m6A-ftz-Δi-5′SS* respectively. Note that one DRACH motif,
139 present near the consensus 5′SS motif, was not altered. When the *ftz-Δi-5′SS* reporter was
140 expressed in human osteosarcoma cell lines (U2OS), elimination of most DRACH motifs
141 drastically reduced m6A deposition (Figure 2B). When the distribution of the mRNAs produced
142 from these various reporters was assessed by RNA fluorescent in situ (FISH) hybridization, we
143 found that although the presence of an intact 5′SS motif promoted nuclear retention, elimination
144 of most DRACH motifs inhibited this retention (Figure 2C-D). Elimination of the DRACH
145 motifs in *ftz-Δi* had no effect on its export. When we expressed versions of *ftz-Δi* and *ftz-Δi-5′SS*
146 mRNA with optimized DRACH motifs (AGACT) to enhance methylation (creating *e-m6A-ftz-Δi*
147 and *e-m6A-ftz-Δi-5′SS*; Figure 2A), we did not observe a significant change in their distribution
148 (Figure 2D).

149

150 **The m6A methyltransferase, METTL3, is required for the nuclear retention of mRNAs**
151 **with an intact 5′SS motif**

152 Next, we tested whether the small molecule STM2457, which sterically blocks the S-
153 adenosylmethionine-binding site of METTL3 and inhibits its RNA methylation activity
154 (Yankova et al. 2021), also inhibited nuclear retention of mRNA with intact 5′SS motifs. When
155 U2OS cells were treated with 100 μM STM2457 for 18 hours, *ftz-Δi-5′SS* mRNA was no longer
156 nuclear retained when compared to DMSO-treated cells (Figure 2E-F). Note that STM2457-
157 treatment had no effect on the nuclear export of *ftz-Δi* mRNA (Figure 2E-F) and minimal effects
158 on the levels of ZFC3H1, YTHDC1, YTHDC2 or U1-70K (Figure S2A-B).

159 To further confirm this result, we depleted METTL3 using a combination of four
160 lentiviral-delivered shRNAs (Figure 3G). We found that in METTL3-depleted cells, *ftz-Δi-5′SS*
161 mRNA was more cytoplasmic than in cells treated with control shRNA (Figure 3H-I). Again, the
162 nuclear export of *ftz-Δi* mRNA was not affected.

163 In aggregate, these results demonstrate that the m6A modification is required for the
164 nuclear retention of reporter mRNAs containing intact 5′SS motifs.

165

166 **YTHDC1 and YTHDC2 are required for the nuclear retention of 5′SS motif containing**
167 **reporter mRNAs**

168 To test whether YTHDC1 and YTHDC2 are required for the nuclear retention of mRNAs
169 with intact 5′SS motifs, we co-depleted these two proteins (Figure 3A) using two lentivirus-
170 delivered shRNAs for each gene. In parallel, we depleted ZFC3H1, which is required for the

171 retention of mRNAs with intact 5′SS motifs (Lee et al. 2022), and ALKBH5, an m6A
172 demethylase (results described in the next section; Figure 3A).

173 We observed that in YTHDC1/2-co-depleted cells, *ftz-Δi-5′SS* mRNA was no longer
174 efficiently retained in the nucleus when compared to control shRNA-treated cells (Figure 3B-C).
175 The degree to which nuclear retention was inhibited was similar to ZFC3H1-depleted cells
176 (Figure 3B-C). Both YTHDC1/2-co-depletion and ZFC3H1-depletion had no effect on the
177 nuclear export of our reporter mRNAs that lacked either the 5′SS motif (*ftz-Δi*) or most DRACH
178 motifs (*no-m6A-ftz-Δi-5′SS*; Figure 3C). Note that YTHDC1/2-depletion had some effect on the
179 levels of ZFC3H1, and vice versa (Figure S3A-B).

180 Next, to validate our results with more natural IPA-generating genes, we monitored IPA
181 transcripts generated from two mini genes, *PCF11-IPA* and *CCDC71-IPA* (Figure 3D-F, S3C-E),
182 that we had previously characterized (Lee et al. 2022). Both reporters are based on endogenous
183 IPA transcripts and require both ZFC3H1 and U1-70K for their efficient nuclear retention. These
184 IPA transcripts can then be specifically monitored by FISH using fluorescent probes that
185 hybridize to the intronic region, just upstream of the 3′ cleavage/polyadenylation site (Figure 3D,
186 S3C). In agreement with our previous results, the two reporters were more cytoplasmic in cells
187 co-depleted of YTHDC1 and YTHDC2 when compared to cells treated with control shRNA
188 (Figure 3E-F, S3D-E).

189 To examine the effects on endogenous IPA transcripts, we fractionated U2OS cells
190 (Figure S3F) that were treated with various shRNAs and assessed the levels of endogenously
191 generated *PCF11* IPA transcripts by qRT-PCR. Depletion of either ZFC3H1 or YTHDC1/2
192 caused an increase in the total levels and in the cytoplasmic/nuclear ratios of endogenous *PCF11*

IPA transcripts (Figure 3G-H), although depletion of the former had a greater effect than depletion of the latter.

Collectively, these results suggest that YTHDC1 and YTHDC2 are required for the efficient nuclear retention of mRNAs with intact 5′SS motifs.

Depletion of the m6A demethylase ALKBH5 inhibits nuclear retention of mRNAs with intact 5′SS motifs

We reasoned that depletion of enzymes that remove the m6A modification should enhance the nuclear retention of transcripts with intact 5′SS motifs. To test this, we depleted ALKBH5 in U2OS cells using lentiviral delivered shRNAs (Figure 3A). Note that due to the nature of our surprising results (see below) we used two different shRNAs to ensure that our findings were not due to off target effects.

Unexpectedly, we found that depletion of ALKBH5 inhibited the nuclear retention of *ftz-Δi-5′SS* mRNA (Figure 3B-C), *PCF11-IPA* (Figure 3E-F) and to a lesser extent *CCDC71-IPA* (Figure S3D-E). Depletion of ALKBH5 had no effect on the nuclear export of our reporter mRNAs that lacked either the 5′SS motif (*ftz-Δi*) or DRACH motifs (*no-m6A-ftz-Δi-5′SS*) (Figure 3B-C). Consistent with previous reports (Zheng et al. 2013), we found that ALKBH5 was present in the nuclear fraction, although it was also present in the cytoplasm (Figure S3G).

From these results, we concluded that ALKBH5 was required for the efficient nuclear retention of most mRNAs that contained intact 5′SS motifs. Although this result seems counter to our other findings, it may indicate that ALKBH5 may play additional roles beyond removing m6A modifications (see discussion).

215

216 **m6A accumulates in IPA transcripts**

217 We next asked whether m6A methylation marks accumulate within natural IPA
218 transcripts. We analyzed CLIP-seq experiments which used an m6A-specific antibody to enrich
219 for modified RNAs isolated from HEK293 cells. We compared the distribution of these m6A
220 methylation marks in intronic regions that have been previously shown to generate IPA
221 transcripts which are sensitive to ZFC3H1-depletion (Lee et al. 2022). As a comparison, each
222 IPA transcript was randomly matched with an exon that was both length- and expression-
223 matched as determined by high throughput sequencing. This matching process was repeated five
224 times across two separate transcriptome sequencing experiments. Although we observed that the
225 average number of m6A modifications per RNA was similar between the IPA transcripts and the
226 length/expression-matched exons (Figure 4A), significantly fewer IPA transcripts lacked
227 detectable m6A modifications (Figure 4B) and significantly more IPA transcripts had a low
228 number of detectable m6A modifications (1-6 sites) when compared to length/expression-
229 matched exons. In contrast, significantly fewer IPA transcripts had a high number of m6A
230 modifications (>12 sites) when compared to length/expression-matched exons (Figure 4B).

231 When the density of m6A modifications was averaged along the length of the intronic
232 portion of IPA transcripts, we found that these m6A marks were slightly enriched near the start of
233 the IPA (i.e., near the 5′SS motif) and near the 3′cleavage/polyadenylation site, when compared
234 to the density of m6A averaged along all exons, where m6A was depleted at both ends near
235 exon-exon boundaries (Figure 4C) as seen by other groups (Yang et al. 2022; Uzonyi et al. 2023;
236 He et al. 2023; Luo et al. 2023). When we looked more closely at three example genes that
237 generate IPA transcripts, *PCF11*, *CSNK1E*, and *NCOA5,* we found that m6A marks were present

238 throughout the intronic region that generates the IPA transcript (Figure 4D-F). In some cases, as
239 in the *NCOA5* IPA transcript, there were only a few m6A marks, but these tended to be near one
240 of the ends of the IPA transcript and also present in the upstream exon. Note that the level of all
241 these IPA transcripts increase in ZFC3H1-depleted U2OS cells (Figure 4D-F) as previously
242 reported (Lee et al. 2022).

243

244 **mRNAs with intact 5′SS motifs accumulate in nuclear foci containing YTHDC1 and this**
245 **requires DRACH motifs**

246 Previously, we found that 5′SS motif containing mRNAs are targeted and then retained in
247 nuclear foci and that their nuclear retention requires nuclear speckles (Lee et al. 2015, 2022). We
248 also found that ZFC3H1 and U1-70K are dispensable for the targeting of these mRNAs to
249 nuclear speckles but instead prevent these RNAs from exiting nuclear foci (Lee et al. 2022).
250 With this in mind, we asked if m6A modifications affect the trafficking of mRNAs in and out of
251 nuclear foci.

252 To determine the localization of mRNAs at early time points post-synthesis, plasmids
253 containing *ftz-Δi-5'SS* and *no-m6A-ftz-Δi-5'SS* reporter genes were microinjected into the nuclei
254 of U2OS cells to allow for rapid synchronous expression. After allowing for one hour of mRNA
255 expression, a time point when nuclear speckle targeting is highest (Akef et al. 2013), cells were
256 fixed and immunostained for SC35, a nuclear speckle marker (Spector et al. 1991) and probed
257 for *ftz* mRNA by FISH. We observed robust nuclear speckle targeting of both constructs (Figure
258 5A-B). This result indicated that within the context of *ftz-Δi-5'SS*, m6A was not required for
259 nuclear speckle targeting.

260 Next, we assessed whether m6A affected the trafficking of mRNAs with intact 5′SS
261 motifs out of nuclear speckles. We thus monitored the mRNA distribution 24h after transfection
262 of the plasmids with reporter genes. At this time point, the distribution of the reporter mRNA
263 reaches steady state and localization in foci is dictated by the rates of entry and egress (Akef et
264 al. 2013). In these cells, *ftz-Δi-5′SS* was mostly localized in foci that contained YTHDC1 (Figure
265 5C, see arrows in the first row). These foci were adjacent to nuclear speckles. When *no-m6A-ftz-*
266 *Δi-5′SS* mRNA was visualized, we observed a slight but consistent colocalization with the
267 nuclear speckle marker SC35, despite the fact that this mRNA was well exported (Figure 5C).
268 There was a lower level of colocalization between this mRNA and YTHDC1. These trends were
269 confirmed by Pearson correlation analysis (Figure 5D). These results indicate that m6A promotes
270 the transfer of mRNAs from nuclear speckles to nearby YTHDC1-containing nuclear foci
271 (Figure 5E).

272

273

Discussion

Here we show that m6A modifications and the m6A binding proteins, YTHDC1 and YTHDC2, are required for the nuclear retention of mRNAs containing intact 5′SS motifs. Moreover, we find that the m6A-binding proteins YTHDC1 and YTHDC2 associate with ZFC3H1 and U1-70K. It is thus likely that these factors form a complex that targets these misprocessed mRNAs for nuclear retention and possibly degradation by the nuclear exosome, which is known to receive substrate RNAs from the PAXT complex. Recent work has demonstrated that m6A modifications are excluded from regions surrounding exon-exon splice site junctions by the exon-junction complex (EJC) (Yang et al. 2022; Uzonyi et al. 2023; He et al. 2023; Luo et al. 2023). Thus, m6A modifications accumulate on unprocessed or misprocessed RNAs, and in conjunction with intact 5′SS motifs, recruit ZFC3H1 to promote RNA nuclear retention and decay (Figure 5E). Furthermore, our findings suggest that mRNAs with 5′SS are first targeted to nuclear speckles, and then transferred to YTHDC1-enriched foci, a nuclear structure that has been likely documented by other groups (Silla et al. 2018; Wang et al. 2021; Cheng et al. 2021).

Our new results suggest that m6A modifications act as a layer of quality control to suppress the expression of unwanted transcripts. Previous reports have implicated m6A in promoting mRNA export, and this is partially based on the analysis of ALKBH5-depletion, which we believe has indirect effects on mRNA metabolism. More recent publications have found that m6A acts as a repressive mark both in terms of nuclear export (Smalec et al. 2022; Tang et al. 2024), RNA stability (Liu et al. 2020) and even feedback to silence chromatin regions that produce transposable element-derived RNA (Chen et al. 2021; Liu et al. 2021). One of the reports that linked m6A to mRNA nuclear export also observed that upon the co-depletion of

297 METTL3 and METTL14 there was a large increase in the cytoplasmic accumulation of m6A-
298 modified mRNAs, suggesting that m6A actually represses nuclear mRNA export (Roundtree et
299 al. 2017). Other studies have found that when m6A modified mRNAs are in the cytoplasm, they
300 are targeted for decay by UPF1 and the CCR4-NOT deadenylase complex, and this may
301 represent a fail-safe mechanism to ensure the silencing of any m6A-enriched RNA that leaks out
302 of the nucleus (Wang et al. 2014; Du et al. 2016; Boo et al. 2022).

303 One unresolved question is why the depletion of ALKBH5 promoted the export of IPA
304 transcripts. One possible explanation is that ALKBH5-depletion disrupted nuclear speckles, as
305 previously reported (Zheng et al. 2013), which are required for the retention of reporter mRNAs
306 with intact 5′SS motifs (Lee et al. 2022). When we stain ALKBH5-depleted U2OS cells for the
307 nuclear speckle marker SC35, we do not see any obvious changes in nuclear speckles (data not
308 shown). Nevertheless, it is possible that ALKBH5-depletion alters some property of speckles that
309 is not obvious by gross inspection of SC35 immunofluorescence. Another possible explanation is
310 that there is some compensatory effect in ALKBH5-depleted cells by the other demethylases
311 (FTO and perhaps ALKBH3), but this needs to be tested.

312 Finally, our results strongly indicate that links between the m6A recognition proteins (i.e.
313 YTH domain containing proteins) and the PAXT complex are evolutionarily conserved. In both
314 humans and *S. pombe*, YTH domain containing proteins appear to be involved in suppressing
315 transposable element-derived RNAs, suggesting additional conserved features. In *S. pombe*, both
316 the MTREC complex and Mmi1 act together to degrade meiotic mRNAs that are inappropriately
317 expressed in interphase cells. MTREC and Mmi1 are bridged by Erh1, which has a human
318 homolog, ERH, that has been recently shown to regulate the stability of transposable element-
319 derived RNAs and meiotic mRNAs (McCarthy et al. 2021). Thus, it is likely that many aspects

of the MTREC-Mmi1 pathway in *S. pombe* are conserved in humans, and our latest results further confirm this idea. Future experiments need to be performed to determine whether other aspects of MTREC and Mmi1 function, including their regulation by TOR signalling and their ability to stimulate heterochromatin formation (Vo et al. 2019; Wei et al. 2021) are conserved in human cells.

Material and Methods

Plasmids constructs and antibodies

All plasmids for reporter constructs in pcDNA3.0, pcDNA3.1 (V5-His) or pcDNA5 are as previously described (Akef et al. 2013; Lee et al. 2015, 2020, 2022; Palazzo et al. 2007). For full length FLAG-ZFC3H1-HA, an insert within the previously published plasmid (FLAG-ZFC3H1 (1-1233)) was deleted by PCR. The *no-m6A-ftz* and *e-m6A-ftz* reporters were synthesized and inserted in pUC57 plasmids (Genscript), subcloned using HindIII and SmaI sites and inserted into pcDNA3.0 or pcDNA3.1 (V5-His) respectively. The FLAG-HA-tagged YTHDC1 plasmid was purchased from Addgene (plasmid # 85167).

Antibodies used in this study include rabbit polyclonals against FLAG (Sigma, F7425), METTL3 (ABclonal, A8370), YTHDC1 (Abcam, ab122340), YTHDC2 (Abcam, ab176846), ALKBH5 (Atlas Antibodies, HPA007196), ZFC3H1 (Bethyl laboratories, A301-457A), U1-70K (Abcam, ab83306), ALY (Zhou et al. 2000), G3BP2 (Proteintech, 16276-1-AP), HA (Sigma, SAB4300), Lamin B1 (Abcam, ab16048), eIF4AIII (generous gift from Dr. Lykke-Anderson's lab), TRAP-α (Görlich et al. 1990), and mouse monoclonals against SC35 (Sigma, Clone 35), FG-nucleoporins (Sigma, mAb414) and α-tubulin (Sigma, DM1A). Immunofluorescence was performed with Alexa647-conjugated secondaries (ThermoFisher) and HRP-conjugated secondaries (Cell Signaling). All antibodies were diluted 1:1000 to 1:2000 for western blotting.

Cell culture, DNA transfection, cell fractionation, and METTL3 inhibition by STM2457

U2OS and HEK293T cells were grown in DMEM media (Wisent) supplemented with 10% fetal bovine serum (FBS) (Wisent) and 5% penicillin/streptomycin (Wisent). DNA

transfection experiments were performed as previously described (Akef et al. 2013; Lee et al. 2015, 2020, 2022; Palazzo et al. 2007). U2OS and HEK cells were transfected with the appropriate amount of DNA plasmid according to the manufacturer's protocol using GenJet U2OS or Lipo293T DNA *in vitro* transfection reagent (SignaGen Laboratories) for 18 to 24 hrs.

Cell fractionation was performed as previously described (Lee et al. 2020). Equivalent amounts of nuclear and cytoplasmic lysates were analysed.

For METTL3 inhibition by STM2457, U2OS cells were transfected with the appropriate plasmids as described above. 6h post-transfection, cells were treated with 100 µM STM2457 (Sigma-Aldrich) or in DMSO for 18h. Cells were fixed and fluorescent in situ hybridization was performed as described below.

Fluorescent in situ hybridization (FISH) staining, immunostaining and analysis of nuclear speckle targeting

Fluorescent in situ hybridization and immunostaining were performed as previously described (Gueroussov et al. 2010; Lee et al. 2015, 2020, 2022).

Analysis of nuclear speckle targeting (Figure 5B) was performed as previously described (Akef et al. 2013). Each analysed region of interest consists of a rectangular region drawn to cover a single SC35-positive speckle and its surroundings (1–4 μm^2). Note that individual nuclear speckles were categorized using Pearson correlation intervals of 0.1, from strongest (Pearson correlation of 1 to 0.9) to weakest (Pearson correlation of 0.6 to 0.5). Any Pearson correlation < 0.5 was scored as "not localized". Analysis of RNA foci (Figure 5D) was similarly performed except that each analysed region of interest consists of a rectangular region drawn to

cover an RNA foci and its surroundings (1–4 μm^2) and Pearson correlation between the RNA and either SC35 or YTHDC1 was tabulated.

Lentiviral delivered shRNA protein depletion

The lentiviral delivered shRNA protein depletion was performed as previously described (Akef et al. 2013; Lee et al. 2015, 2020, 2022; Palazzo et al. 2007). HEK293T were plated at 50% confluency on 60 mm dishes and transiently transfected with the gene specific shRNA pLKO.1 plasmid (Sigma), packaging plasmid (Δ8.9) and envelope (VSVG) vectors using Lipo293T DNA *in vitro* transfection reagent (SignaGen Laboratories) according to the manufacture's protocol. Viruses were harvested from the media 48 h post-transfection and added to U2OS cells pre-treated with 8 μg/ml hexadimethrine bromide. Cells were selected with 2 μg/ml puromycin media for at least 4 to 6 days. Western blotting was used to determine the efficiency of YTHDC1/YTHDC2, METTL3, ALKBH5 and ZFC3H1 depletion. The shRNAs constructs (Sigma) used in this study are as follows: **ZFC3H1-2** "TRCN0000432333" 5'-CCGGGACTGA TGACATCGCT AATTTCTCGA GAAATTAGCG ATGTCATCAG TCTTTTTTG-3', **YTHDC1-1** "TRCN0000243987" 5'- CCGGTGGATT TGCAGGCGTG AATTACTCGA GTAATTCACG CCTGCAAATC CATTTTTG -3', **YTHDC1-2** "TRCN0000243988" 5'-CCGGCACCAG AGACCAGGGT ATTTACTCGA GTAAATACCC TGGTCTCTGG TGTTTTTG -3', **YTHDC2-1** "TRCN0000157638" 5'-CCGGCGGAAG CTAAATCGAG CCTTTCTCGA GAAAGGCTCG ATTTAGCTTC CGTTTTTTG-3', **YTHDC2-2** "TRCN0000232759" 5'-CCGGCAGAAG TGGCATAGCT TATTTCTCGA GAAATAAGCT ATGCCACTTC TGTTTTTG -3', **ALKBH5-1** "TRCN0000064783" 5'-CCGGG AAAGG CTGTTGGCAT CAATACTCGA GTATTGATGC CAACAGCCTT

TCTTTTTG-3', **ALKBH5-2** "TRCN0000064787" 5'-CCGGCCTCAG GAAGACAAGA TTAGACTCGA GTCTAATCTT GTCTTCCTGA GGTTTTTG-3', **METTL3-1** "TRCN0000034714" 5'-CCGGGCCTTA ACATTGCCCA CTGATCTCGA GATCAGTGGG CAATGTTAAG GCTTTTTG-3', **METTL3-2** "TRCN0000034717" 5'- CCGGGCCAAG GAACAATCCA TTGTTCTCGA GAACAATGGA TTGTTCCTTG GCTTTTTG-3', **METTL3-3** "TRCN0000289743" 5'-CCGGGCAAGT ATGTTCACTA TGAAACTCGA GTTTCATAGT GAACATACTT GCTTTTTG-3', **METTL3-4** "TRCN0000289812" 5'-CCGGCGTCAG TATCTTGGGC AAGTTCTCGA GAACTTGCCC AAGATACTGA CGTTTTTG-3'.

FLAG co-immunoprecipitation

FLAG co-immunoprecipitation was performed as previously described (Lee et al. 2022), except with these modifications. 1X 150 mm dish of HEK293 cells were transfected with either FLAG-HA-YTHDC1, FLAG-ZFC3H1-HA or FLAG-ZFC3H1 (1-1233) using Lipo293T DNA *in vitro* transfection reagent according to manufacturer's instructions (SignaGen Laboratories). 18 to 24h post transfection the cell pellets were trypsinized, collected and washed with 3 times with in ice-cold 1X PBS and flash frozen in liquid nitrogen. In parallel, another 150 mm dish of untransfected HEK293 cells of similar confluency was collected. The pellets were lysed in 2 ml lysis buffer (20 mM Tris-HCl, pH 8, 137 mM NaCl, 1% NP-40, 2 mM EDTA and *cOmplete* mini-protease inhibitor (Roche)) for 10 min rocking on a nutator at 4 °C. To ensure that the nuclear proteins were released from chromatin, the lysed sample was passed through a 25¾″ needle 5X times to shear the chromatin before incubation. The lysate was cleared by spinning at 16,100*g* for 10 min. ~950 µl of the lysate was added to ~50 to 60 µl FLAG M2 beads (Sigma-

Aldrich, A2220), previously preincubated overnight with 5% BSA and 667 µg/ml Ultra-Pure salmon sperm DNA (Invitrogen), and incubated for 3h or overnight at 4 °C. The remaining ~50 µl of the lysate was reserved as "INPUT", and 5X sample buffer was added and the sample was boiled at 95°C for 5 min. Following incubation, the FLAG M2 beads was washed 2 to 5 times with 300 mM wash buffer (20 mM Tris-HCl, pH 8, 300 mM NaCl, 0.05% NP-40, 2 mM EDTA and *cOmplete* mini-protease inhibitor (Roche)), one time with 137 mM wash buffer (same as for 300 mM wash buffer, except with 137 mM NaCl) and transferred to a new Eppendorf tube. Subsequently, for RNase digested samples, ~400µl of 1:1000 RNase A/T1 (Thermo Scientific, EN055) diluted in 137 mM wash was added to the FLAG M2 beads and incubated for 20 min at 4°C. Samples that were not RNase digested were treated in the same manner, except the RNase A/T1 was omitted in the incubation mixture. The samples were washed twice with 137 mM wash buffer, transferred to a new Eppendorf tube and 50 to 100 µl 2.5X sample buffer was added to sample and boiled a 95°C for 5 min. Samples were separated on an SDS-PAGE gel and transferred onto a blot for immunoblotting.

RNaseA/T1 treatment

The RNase efficacy in our co-immunoprecipitation experiments was validated by showing the loss of RNA integrity upon RNase treatment using a denaturing agarose gel. The co-immunoprecipitate lysate was treated with or without RNaseA/T1 followed by RNA extraction by Trizol extraction, followed by isopropanol precipitation. RNA samples were denatured using formamide and formaldehyde in MOPS buffer and incubated at 65°C for 30 min. Denatured RNA was run on an agarose gel supplemented with formaldehyde and stained with SYBR Gold. Integrity was assessed by visualizing the presence of intact 28S and 18S rRNA bands in the gel.

m6A-miCLIP-seq

miCLIP-seq was performed as previously described (Linder et al. 2015), with modifications as detailed below. Briefly, cells were grown in independent batches to represent biological replicates. We extracted total RNA from HEK293 cells using TRIzol according to manufacturer's instructions. After RNA was treated with DNase I, 12 µg of total RNA was used for miCLIP-seq. 2 µl of RNA Fragmentation Reagents (Invitrogen AM8740) was added to the RNA suspended in 20 µl of sterile water. The mixture was incubated in a heat block at 75°C for exactly 12 minutes. Reaction was stopped by adding 2 µl of stop solution (Invitrogen AM8740). The fragmented RNA was incubated with 10 µg of m6A antibody (MBL RN131P) for 2 hours at 4°C. RNA-antibody complexes were UV crosslinked twice with 0.15 J/cm^2 at 254 nm in a Stratalinker 1800. 100µl of Protein G Dynabeads were added, and the samples were rotated for 2 hours at 4°C. Samples were washed three times using iCLIP high salt buffer with 5 min rotation in the cold room for each wash. RNA dephosphorylation was performed using FastAP and T4 polynucleotide kinase. Pre-adenylated L3 adaptors were ligated to the 3′ends of RNAs using the enhanced CLIP ligation method, as detailed previously (Nabeel-Shah and Greenblatt 2023). RNA was 5’-end-labeled with ^{32}P using T4 polynucleotide kinase (New England Biolabs catalogue number M0201L). Samples were separated using 4–12% BisTris-PAGE and transferred to a nitrocellulose membrane (Protran). RNA was recovered from the membrane by digesting proteins with proteinase K (Thermo Fisher catalogue number 25530049). Recovered RNA was reverse transcribed into cDNA using barcoded iCLIP primers. The cDNA was size-selected (low: 70 to 85 nt, middle: 85 to 110 nt, and high: 110 to 180 nt) using 6% TBE-Urea gels. cDNA was circularized using CircLigase™ II ssDNA ligase to add the adaptor to the 5’-end. We added betain at a final concentration of 1 M in the reaction and mixture was incubated

for 2 hours at 60°C, as detailed previously (Nabeel-Shah and Greenblatt 2023). Circularized cDNA was digested at the internal BamHI site for linearization. Linearized cDNA was PCR amplified using Phusion High-Fidelity PCR Master Mix (NEB, M0531S).

The final PCR libraries were agarose gel purified on purification columns (QIAGEN). The eluted DNA was mixed at a ratio of 1:5:5 from the low, middle, and high fractions and submitted for sequencing on an Illumina NextSeq 500 platform to obtain single-end 51 nucleotide reads with 40 million read depth per sample. miCLIP-seq data is deposited at Gene Expression Omnibus (GEO, https://www.ncbi.nlm.nih.gov/geo/) with the accession code GSE230846 for the series, which contains several other datasets submitted as a part of Nabeel-Shah et al. (under review).

miCLIP-seq analysis

miCLIP-seq analyses were performed as detailed in our previous reports for iCLIP-seq (Song et al. 2022). Briefly, 51-nt miCLIP-seq raw reads that consist of 3 random positions, a 4-nt multiplexing barcode, and another 2 random positions, followed by the cDNA sequence were de-duplicated based on the first 45 nt, and random positions, barcodes, and any 3′-bases matching Illumina adaptors were removed. Reads shorter than 25 nt were discarded, and the remaining reads were trimmed to 35nt using Trimmomatic (Bolger et al. 2014). Reads were mapped to the human genome/transcriptome (Ensembl annotation hg19) using Tophat (Trapnell et al. 2009) with default settings where reads with a mapping quality < 3 were removed from further analysis, which also removes multi-mapping reads.

Crosslinked induced truncations (CITS)

The precise m6A site was inferred by identifying m6A antibody crosslink induced truncation sites, due to the fact that reverse transcriptase does not efficiently transcribe across crosslinked regions. CLIP Tool Kit (CTK) was used to identify RNA-binding sites at single-nucleotide resolution (Shah et al. 2017). As miCLIP-seq aims to capture the crosslink-induced truncation sites (CITS) during cDNA preparation, we therefore called CITS, rather than CIMS (crosslink-induced mutations), on individual replicates. CITS with FDR ≤ 0.01 were considered as significant. CITS from 2 replicates were merged at a maximum gap of 1 bp. Each peak was then extended 2 bp both upstream and downstream of the identified CITS. Subsequently, only those CITS with a DRACH motif were selected and the coordinates of the base 'A' in the motif were designated as m6A sites.

Bioinformatic analysis of m6A density and distribution in IPA transcripts

A list of introns that do not overlap with exons on the opposite strand was compiled from Gencode v.19. To identify ZFC3H1-regulated IPA transcripts, intronic reads from shZFC3H1 U2OS Frac-Seq data (Lee et al. 2022) were analysed using rtracklayer (Lawrence et al. 2009) to identify introns with enrichment in the first 20% over the last 20%. Next, introns with more overall reads in shZFC3H1 compared to shControl conditions were selected. IPA 5' splice sites were inferred from the PolyA feature annotation file from Gencode.

To estimate the levels of IPA transcripts compared to exons in HEK293 cells, previously published RNAseq data (GEO: GSE165772) was aligned to the Ensemble GRCh38 genome by STAR (Dobin et al. 2013). Samtools (Danecek et al. 2021) coverage command was used to obtain the RNAseq coverage (meandepth column) at all the unique IPA transcripts and exon sites. To compare relative m6A levels each IPA transcripts was randomly matched with an exon

499 that was both size matched (in nucleotide length, allowing for +/- 10% difference) and
500 expression matched (mean read depth, allowing for +/- 10% difference). Average m6A reads per
501 IPA transcripts or exon were compiled. The IPA transcript-exon matching procedure was
502 repeated five times, to determine whether differences were statistically significant. This entire
503 procedure was then repeated using two separate RNAseq runs (GSM5049715 and
504 GSM5049716). It should be noted that many IPAs are present at extremely low levels and this
505 likely impeded our ability to detect m6A sites; however, this is equally true for the expression-
506 matched exon group.

507 To determine the distribution of m6A reads from the miCLIP analysis along IPA
508 transcripts and exonic regions, m6A peaks were aligned to IPAs or exons using their genomic
509 coordinates and normalized to the length of the IPA or exon. The distribution was plotted using
510 the ggplot2 density geometry (Wickham 2009). Most bioinformatical analyses were done using
511 R Statistical Software v4.2.2 (R Core Team 2022).

512

513 **Research Contributions**

514 E.S.L., H.W.S., Y.E.W, S.S.J.I., L.S.O. and N.S.K., performed the experiments under the
515 guidance of A.F.P.. R.E.J. and Y.L.L. performed the bioinformatics analysis of m6A distribution
516 under the guidance of A.F.P.. S.N.S performed the m6A-miCLIP experiments and S.P. performed
517 the bioinformatics analysis under the guidance of J.F.G.. E.S.L. and A.F.P. co-wrote the paper,
518 with input from all other authors.

519

520 **Funding**

This work was supported by a grant to AFP from Natural Sciences and Engineering Research Council of Canada (FN 492860).

Conflict of Interest

The authors have declared that no conflict of interest exists.

Acknowledgements

We thank members of the Donnelly Centre RNA sequencing facility for performing the m6A-miCLIP RNA sequencing. We thank G. L. Burke and N. Ahmed, for assistance with the m6A-miCLIP library preparation, J. Gao for her helpful discussions for the bioinformatics analysis and W.S. Tse for his technical expertise for our computational needs. Finally, we thank members of the Palazzo lab for their helpful discussions and insights.

References

Abad X, Vera M, Jung SP, Oswald E, Romero I, Amin V, Fortes P, Gunderson SI. 2008. Requirements for gene silencing mediated by U1 snRNA binding to a target sequence. *Nucleic Acids Res* **36**: 2338–2352.

Akef A, Zhang H, Masuda S, Palazzo AF. 2013. Trafficking of mRNAs containing ALREX-promoting elements through nuclear speckles. *Nucleus* **4**: 326–340.

Bolger AM, Lohse M, Usadel B. 2014. Trimmomatic: a flexible trimmer for Illumina sequence data. *Bioinformatics* **30**: 2114–2120.

Boo SH, Ha H, Lee Y, Shin M-K, Lee S, Kim YK. 2022. UPF1 promotes rapid degradation of m6A-containing RNAs. *Cell Reports* **39**: 110861.

544 Chen C, Liu W, Guo J, Liu Y, Liu X, Liu J, Dou X, Le R, Huang Y, Li C, et al. 2021. Nuclear m6A reader YTHDC1
545 regulates the scaffold function of LINE1 RNA in mouse ESCs and early embryos. *Protein Cell* **12**:
546 455–474.

547 Chen H-M, Futcher B, Leatherwood J. 2011. The fission yeast RNA binding protein Mmi1 regulates
548 meiotic genes by controlling intron specific splicing and polyadenylation coupled RNA turnover.
549 *PLoS One* **6**: e26804.

550 Cheng Y, Xie W, Pickering BF, Chu KL, Savino AM, Yang X, Luo H, Nguyen DTT, Mo S, Barin E, et al. 2021.
551 N6-Methyladenosine on mRNA facilitates a phase-separated nuclear body that suppresses
552 myeloid leukemic differentiation. *Cancer Cell* **39**: 958-972.e8.

553 Danecek P, Bonfield JK, Liddle J, Marshall J, Ohan V, Pollard MO, Whitwham A, Keane T, McCarthy SA,
554 Davies RM, et al. 2021. Twelve years of SAMtools and BCFtools. *GigaScience* **10**: giab008.

555 Dobin A, Davis CA, Schlesinger F, Drenkow J, Zaleski C, Jha S, Batut P, Chaisson M, Gingeras TR. 2013.
556 STAR: ultrafast universal RNA-seq aligner. *Bioinformatics* **29**: 15–21.

557 Dominissini D, Moshitch-Moshkovitz S, Schwartz S, Salmon-Divon M, Ungar L, Osenberg S, Cesarkas K,
558 Jacob-Hirsch J, Amariglio N, Kupiec M, et al. 2012. Topology of the human and mouse m6A RNA
559 methylomes revealed by m6A-seq. *Nature* **485**: 201–206.

560 Du H, Zhao Y, He J, Zhang Y, Xi H, Liu M, Ma J, Wu L. 2016. YTHDF2 destabilizes m(6)A-containing RNA
561 through direct recruitment of the CCR4-NOT deadenylase complex. *Nat Commun* **7**: 12626.

562 Fortes P, Cuevas Y, Guan F, Liu P, Pentlicky S, Jung SP, Martínez-Chantar ML, Prieto J, Rowe D, Gunderson
563 SI. 2003. Inhibiting expression of specific genes in mammalian cells with 5' end-mutated U1
564 small nuclear RNAs targeted to terminal exons of pre-mRNA. *Proc Natl Acad Sci USA* **100**: 8264–
565 8269.

566 Garland W, Jensen TH. 2020. Nuclear sorting of RNA. *WIREs RNA* **11**: e1572.

567 Goraczniak R, Behlke MA, Gunderson SI. 2009. Gene silencing by synthetic U1 adaptors. *Nat Biotechnol*
568 **27**: 257–263.

569 Görlich D, Prehn S, Hartmann E, Herz J, Otto A, Kraft R, Wiedmann M, Knespel S, Dobberstein B,
570 Rapoport TA. 1990. The signal sequence receptor has a second subunit and is part of a
571 translocation complex in the endoplasmic reticulum as probed by bifunctional reagents. *J Cell*
572 *Biol* **111**: 2283–2294.

573 Gueroussov S, Tarnawsky SP, Cui XA, Mahadevan K, Palazzo AF. 2010. Analysis of mRNA Nuclear Export
574 Kinetics in Mammalian Cells by Microinjection. *J Vis Exp* **46**: 2387.

575 He PC, Wei J, Dou X, Harada BT, Zhang Z, Ge R, Liu C, Zhang L-S, Yu X, Wang S, et al. 2023. Exon
576 architecture controls mRNA m6A suppression and gene expression. *Science* **379**: 677–682.

577 Ishigami Y, Ohira T, Isokawa Y, Suzuki Y, Suzuki T. 2021. A single m6A modification in U6 snRNA diversifies
578 exon sequence at the 5' splice site. *Nat Commun* **12**: 3244.

579 Jia G, Fu Y, Zhao X, Dai Q, Zheng G, Yang Y, Yi C, Lindahl T, Pan T, Yang Y-G, et al. 2011. N6-
580 methyladenosine in nuclear RNA is a major substrate of the obesity-associated FTO. *Nat Chem*
581 *Biol* **7**: 885–887.

582 Kaida D, Berg MG, Younis I, Kasim M, Singh LN, Wan L, Dreyfuss G. 2010. U1 snRNP protects pre-mRNAs
583 from premature cleavage and polyadenylation. *Nature* **468**: 664–668.

584 Lawrence M, Gentleman R, Carey V. 2009. rtracklayer: an R package for interfacing with genome
585 browsers. *Bioinformatics* **25**: 1841–1842.

586 Lee ES, Akef A, Mahadevan K, Palazzo AF. 2015. The consensus 5' splice site motif inhibits mRNA nuclear
587 export. *PLoS One* **10**: e0122743.

588 Lee ES, Smith HW, Wolf EJ, Guvenek A, Wang YE, Emili A, Tian B, Palazzo AF. 2022. ZFC3H1 and U1-70K
589 promote the nuclear retention of mRNAs with 5' splice site motifs within nuclear speckles. *RNA*
590 **28**: 878–894.

591 Lee ES, Wolf EJ, Ihn SSJ, Smith HW, Emili A, Palazzo AF. 2020. TPR is required for the efficient nuclear
592 export of mRNAs and lncRNAs from short and intron-poor genes. *Nucleic Acids Res* **48**: 11645–
593 11663.

594 Legrain P, Rosbash M. 1989. Some cis- and trans-acting mutants for splicing target pre-mRNA to the
595 cytoplasm. *Cell* **57**: 573–583.

596 Lesbirel S, Viphakone N, Parker M, Parker J, Heath C, Sudbery I, Wilson SA. 2018. The m6A-methylase
597 complex recruits TREX and regulates mRNA export. *Sci Rep* **8**: 13827.

598 Lesbirel S, Wilson SA. 2019. The m6A-methylase complex and mRNA export. *Biochimica et Biophysica*
599 *Acta (BBA) - Gene Regulatory Mechanisms* **1862**: 319–328.

600 Linder B, Grozhik AV, Olarerin-George AO, Meydan C, Mason CE, Jaffrey SR. 2015. Single-nucleotide-
601 resolution mapping of m6A and m6Am throughout the transcriptome. *Nat Methods* **12**: 767–
602 772.

603 Liu J, Dou X, Chen C, Chen C, Liu C, Xu MM, Zhao S, Shen B, Gao Y, Han D, et al. 2020. N6-
604 methyladenosine of chromosome-associated regulatory RNA regulates chromatin state and
605 transcription. *Science* **367**: 580–586.

606 Liu J, Gao M, He J, Wu K, Lin S, Jin L, Chen Y, Liu H, Shi J, Wang X, et al. 2021. The RNA m6A reader
607 YTHDC1 silences retrotransposons and guards ES cell identity. *Nature* **591**: 322–326.

608 Liu J, Yue Y, Han D, Wang X, Fu Y, Zhang L, Jia G, Yu M, Lu Z, Deng X, et al. 2014. A METTL3-METTL14
609 complex mediates mammalian nuclear RNA N6-adenosine methylation. *Nat Chem Biol* **10**: 93–
610 95.

611 Luo Z, Ma Q, Sun S, Li N, Wang H, Ying Z, Ke S. 2023. Exon-intron boundary inhibits m6A deposition,
612 enabling m6A distribution hallmark, longer mRNA half-life and flexible protein coding. *Nat*
613 *Commun* **14**: 4172.

614 McCarthy RL, Kaeding KE, Keller SH, Zhong Y, Xu L, Hsieh A, Hou Y, Donahue G, Becker JS, Alberto O, et al.
615 2021. Diverse heterochromatin-associated proteins repress distinct classes of genes and
616 repetitive elements. *Nat Cell Biol* **23**: 905–914.

617 Meola N, Domanski M, Karadoulama E, Chen Y, Gentil C, Pultz D, Vitting-Seerup K, Lykke-Andersen S,
618 Andersen JS, Sandelin A, et al. 2016. Identification of a Nuclear Exosome Decay Pathway for
619 Processed Transcripts. *Mol Cell* **64**: 520–533.

620 Meyer KD, Saletore Y, Zumbo P, Elemento O, Mason CE, Jaffrey SR. 2012. Comprehensive analysis of
621 mRNA methylation reveals enrichment in 3' UTRs and near stop codons. *Cell* **149**: 1635–1646.

622 Nabeel-Shah S, Greenblatt J. 2023. Revised iCLIP-seq Protocol for Profiling RNA–protein Interaction Sites
623 at Individual Nucleotide Resolution in Living Cells. *BIO-PROTOCOL* **13**: e4688.

624 Nayler O, Hartmann AM, Stamm S. 2000. The ER Repeat Protein Yt521-B Localizes to a Novel Subnuclear
625 Compartment. *J Cell Biol* **150**: 949–962.

626 Ogami K, Manley JL. 2017. Mtr4/ZFC3H1 protects polysomes through nuclear RNA surveillance. *Cell Cycle*
627 **16**: 1999–2000.

628 Ogami K, Richard P, Chen Y, Hoque M, Li W, Moresco JJ, Yates JR, Tian B, Manley JL. 2017. An
629 Mtr4/ZFC3H1 complex facilitates turnover of unstable nuclear RNAs to prevent their cytoplasmic
630 transport and global translational repression. *Genes Dev* **31**: 1257–1271.

631 Palazzo AF, Lee ES. 2018. Sequence Determinants for Nuclear Retention and Cytoplasmic Export of
632 mRNAs and lncRNAs. *Front Genet* **9**: 440.

633 Palazzo AF, Qiu Y, Kang YM. 2024. mRNA nuclear export: how mRNA identity features distinguish
634 functional RNAs from junk transcripts. *RNA Biol* **21**: 1–12.

635 Palazzo AF, Springer M, Shibata Y, Lee C-S, Dias AP, Rapoport TA. 2007. The signal sequence coding region
636 promotes nuclear export of mRNA. *PLoS Biol* **5**: e322.

637 R Core Team. 2022. R: A language and environment for statistical computing. https://www.R-
638 project.org/.

639 Roundtree IA, Luo G-Z, Zhang Z, Wang X, Zhou T, Cui Y, Sha J, Huang X, Guerrero L, Xie P, et al. 2017.
640 YTHDC1 mediates nuclear export of N6-methyladenosine methylated mRNAs. *Elife* **6**: e31311.

641 Shah A, Qian Y, Weyn-Vanhentenryck SM, Zhang C. 2017. CLIP Tool Kit (CTK): a flexible and robust
642 pipeline to analyze CLIP sequencing data. *Bioinformatics* **33**: 566–567.

643 Shichino Y, Otsubo Y, Kimori Y, Yamamoto M, Yamashita A. 2018. YTH-RNA-binding protein prevents
644 deleterious expression of meiotic proteins by tethering their mRNAs to nuclear foci ed. T.H.
645 Jensen. *eLife* **7**: e32155.

646 Shichino Y, Otsubo Y, Yamamoto M, Yamashita A. 2020. Meiotic gene silencing complex MTREC/NURS
647 recruits the nuclear exosome to YTH-RNA-binding protein Mmi1. *PLOS Genetics* **16**: e1008598.

648 Silla T, Karadoulama E, Mąkosa D, Lubas M, Jensen TH. 2018. The RNA Exosome Adaptor ZFC3H1
649 Functionally Competes with Nuclear Export Activity to Retain Target Transcripts. *Cell Rep* **23**:
650 2199–2210.

651 Silla T, Schmid M, Dou Y, Garland W, Milek M, Imami K, Johnsen D, Polak P, Andersen JS, Selbach M, et al.
652 2020. The human ZC3H3 and RBM26/27 proteins are critical for PAXT-mediated nuclear RNA
653 decay. *Nucleic Acids Res* **48**: 2518–2530.

654 Smalec BM, Ietswaart R, Choquet K, McShane E, West ER, Churchman LS. 2022. Genome-wide
655 quantification of RNA flow across subcellular compartments reveals determinants of the
656 mammalian transcript life cycle. 2022.08.21.504696.
657 https://www.biorxiv.org/content/10.1101/2022.08.21.504696v1 (Accessed January 5, 2023).

658 Song J, Nabeel-Shah S, Pu S, Lee H, Braunschweig U, Ni Z, Ahmed N, Marcon E, Zhong G, Ray D, et al.
659 2022. Regulation of alternative polyadenylation by the C2H2-zinc-finger protein Sp1. *Mol Cell* **82**:
660 3135-3150.e9.

661 Spector DL, Fu XD, Maniatis T. 1991. Associations between distinct pre-mRNA splicing components and
662 the cell nucleus. *EMBO J* **10**: 3467–3481.

663 Sugiyama T, Sugioka-Sugiyama R. 2011. Red1 promotes the elimination of meiosis-specific mRNAs in
664 vegetatively growing fission yeast. *EMBO J* **30**: 1027–1039.

665 Sugiyama T, Thillainadesan G, Chalamcharla VR, Meng Z, Balachandran V, Dhakshnamoorthy J, Zhou M,
666 Grewal SIS. 2016. Enhancer of Rudimentary Cooperates with Conserved RNA-Processing Factors
667 to Promote Meiotic mRNA Decay and Facultative Heterochromatin Assembly. *Mol Cell* **61**: 747–
668 759.

669 Tang P, Yang J, Chen Z, Du C, Yang Y, Zhao H, Huang L, Li G, Liu F, Dong B, et al. 2024. Nuclear retention
670 coupled with sequential polyadenylation dictates post-transcriptional m6A modification in the
671 nucleus. *Mol Cell* **84**: 3758-3774.e10.

672 Tian B, Pan Z, Lee JY. 2007. Widespread mRNA polyadenylation events in introns indicate dynamic
673 interplay between polyadenylation and splicing. *Genome Res* **17**: 156–165.

674 Trapnell C, Pachter L, Salzberg SL. 2009. TopHat: discovering splice junctions with RNA-Seq.
675 *Bioinformatics* **25**: 1105–1111.

676 Ueda Y, Ooshio I, Fusamae Y, Kitae K, Kawaguchi M, Jingushi K, Hase H, Harada K, Hirata K, Tsujikawa K.
677 2017. AlkB homolog 3-mediated tRNA demethylation promotes protein synthesis in cancer cells.
678 *Sci Rep* **7**: 42271.

679 Uzonyi A, Dierks D, Nir R, Kwon OS, Toth U, Barbosa I, Burel C, Brandis A, Rossmanith W, Le Hir H, et al.
680 2023. Exclusion of m6A from splice-site proximal regions by the exon junction complex dictates
681 m6A topologies and mRNA stability. *Mol Cell* **83**: 237-251.e7.

682 Veitia RA. 2007. Exploring the Molecular Etiology of Dominant-Negative Mutations. *Plant Cell* **19**: 3843–
683 3851.

684 Vo TV, Dhakshnamoorthy J, Larkin M, Zofall M, Thillainadesan G, Balachandran V, Holla S, Wheeler D,
685 Grewal SIS. 2019. CPF Recruitment to Non-canonical Transcription Termination Sites Triggers
686 Heterochromatin Assembly and Gene Silencing. *Cell Rep* **28**: 267-281.e5.

687 Wang C, Zhu Y, Bao H, Jiang Y, Xu C, Wu J, Shi Y. 2016. A novel RNA-binding mode of the YTH domain
688 reveals the mechanism for recognition of determinant of selective removal by Mmi1. *Nucleic*
689 *Acids Res* **44**: 969–982.

690 Wang X, Lu Z, Gomez A, Hon GC, Yue Y, Han D, Fu Y, Parisien M, Dai Q, Jia G, et al. 2014. m6A-dependent
691 regulation of messenger RNA stability. *Nature* **505**: 117–120.

692 Wang Y, Fan J, Wang J, Zhu Y, Xu L, Tong D, Cheng H. 2021. ZFC3H1 prevents RNA trafficking into nuclear
693 speckles through condensation. *Nucleic Acids Research* **49**: 10630–10643.

694 Wei Y, Lee NN, Pan L, Dhakshnamoorthy J, Sun L-L, Zofall M, Wheeler D, Grewal SIS. 2021. TOR targets an
695 RNA processing network to regulate facultative heterochromatin, developmental gene
696 expression and cell proliferation. *Nat Cell Biol* **23**: 243–256.

697 Wickham H. 2009. *Ggplot2: elegant graphics for data analysis*. Springer, New York.

698 Xu C, Wang X, Liu K, Roundtree IA, Tempel W, Li Y, Lu Z, He C, Min J. 2014. Structural basis for selective
699 binding of m6A RNA by the YTHDC1 YTH domain. *Nat Chem Biol* **10**: 927–929.

700 Xu Y, Zhang W, Shen F, Yang X, Liu H, Dai S, Sun X, Huang J, Guo Q. 2021. YTH Domain Proteins: A Family
701 of m6A Readers in Cancer Progression. *Frontiers in Oncology* **11**: 629560.

702 Yang X, Triboulet R, Liu Q, Sendinc E, Gregory RI. 2022. Exon junction complex shapes the m6A
703 epitranscriptome. *Nat Commun* **13**: 7904.

704 Yankova E, Blackaby W, Albertella M, Rak J, De Braekeleer E, Tsagkogeorga G, Pilka ES, Aspris D, Leggate
705 D, Hendrick AG, et al. 2021. Small-molecule inhibition of METTL3 as a strategy against myeloid
706 leukaemia. *Nature* **593**: 597–601.

707 Zheng G, Dahl JA, Niu Y, Fedorcsak P, Huang C-M, Li CJ, Vågbø CB, Shi Y, Wang W-L, Song S-H, et al. 2013.
708 ALKBH5 Is a Mammalian RNA Demethylase that Impacts RNA Metabolism and Mouse Fertility.
709 *Mol Cell* **49**: 18–29.

710 Zhou Y, Zhu J, Schermann G, Ohle C, Bendrin K, Sugioka-Sugiyama R, Sugiyama T, Fischer T. 2015. The
711 fission yeast MTREC complex targets CUTs and unspliced pre-mRNAs to the nuclear exosome.
712 *Nat Commun* **6**: 7050.

713 Zhou Z, Luo MJ, Straesser K, Katahira J, Hurt E, Reed R. 2000. The protein Aly links pre-messenger-RNA
714 splicing to nuclear export in metazoans. *Nature* **407**: 401–405.

715

716

717 **Figure Legends**

718 **Figure 1. YTHDC1 and YTHDC2 interact with ZFC3H1 and U1-70K**

719 (A) The main components of the MTREC complex (outlined by a dotted line) and associated
720 factors in *S. pombe* (left), and their human homologs, including the PAXT complex (outlined by
721 a dotted line) and YTH proteins (right).

722 (B) HEK293 cells were either transfected with FLAG-tagged YTHDC1 or mock transfected.
723 After 18-24 hours, cell lysates were collected and subjected to immunoprecipitation using FLAG
724 M2 beads. Precipitates were then treated with either buffer or a combination of RNase A and
725 RNase T1 and reisolated to remove RNA-dependent interacting proteins. Samples were
726 separated by SDS-PAGE and immunoblotted for the indicated proteins. Note that the inputs
727 represent 5% of the samples used for immunoprecipitation.

728 (C-D) Similar to (B), except that cells were transfected with FLAG/HA-tagged ZFC3H1 (FLAG-
729 ZFC3H1-HA).

730 (E-F) Similar to (B), except that cells were transfected with a FLAG-tagged fragment of
731 ZFC3H1 containing amino acids 1-1233.

732

733 **Figure 2. The m6A modification is required for nuclear retention of 5′SS motif containing**
734 **mRNAs**

735 (A) Schematic of the intronless fushi-tarazu (*ftz-Δi*) reporters used in this study, with and without
736 the 5′SS motif in the 3′UTR. Note that the consensus 5′SS motif promotes nuclear retention. The

737 positions of either consensus DRACH motifs, or their mutated forms that either eliminate the
738 motifs (AGGCT), or enhance the motifs (AGACT) are indicated.

739 (B) U2OS cells were transfected with the indicated *ftz* reporters. After 18-24 hours, RNA was
740 isolated and immunoprecipitated with anti-m6A antibodies or IgG controls. Levels of *ftz* in the
741 precipitates were assessed by qRT-PCR. Each bar represents the average and standard error of at
742 three independent experiments. Student t-test was performed, * $p < 0.05$ ** $p < 0.01$ *** $p <$
743 0.001.

744 (C-D) U2OS cells were transfected with the indicated *ftz* reporters. 18-24 hours later the cells
745 were fixed and the mRNA was visualized by fluorescent in situ hybridization (FISH) using
746 probes against *ftz*. Representative images are shown in (C), scale bar = 20 µm, and quantification
747 is shown in (D). Each bar represents the average and standard error of at least three independent
748 experiments, each experiment consisting of at least 30 to 60 cells. Student t-test was performed,
749 *** $p < 0.001$.

750 (E-F) U2OS cells were transfected with the indicated *ftz* reporters. 6h post transfection, cells
751 were treated with 100 µM STM2457 or DMSO. 18 hours later, the cells were fixed and the
752 mRNA was visualized by FISH. Representative images are shown in (E), scale bar = 20 µm, and
753 quantification shown in (F). Each bar represents the average and standard error of at least three
754 independent experiments, each experiment consisting of at least 30 to 60 cells. Student t-test was
755 performed, * $p < 0.05$.

756 (G-I) U2OS cells were treated with lentivirus containing four different shRNAs against METTL3
757 or scrambled control shRNA. (G) Lysates were collected after 96 hours, separated by SDS-
758 PAGE, and immunoprobed for METTL3 or tubulin. (H-I) Control- or METTL3-depleted cells

759 were transfected with the indicated *ftz* reporters. 18-24 hours later the cells were fixed and the
760 mRNA was visualized by FISH. Representative images are shown in (H), scale bar = 20 µm, and
761 quantification is shown in (I). Each bar represents the average and standard error of three
762 independent experiments, each experiment consisting of at least 30 to 60 cells. Student t-test was
763 performed, ** $p < 0.01$.

764

765 **Figure 3. YTHDC1/YTHDC2 and ALKBH5 are required for the nuclear retention of 5′SS**
766 **motif containing mRNAs**

767 (A) U2OS cells were treated with different lentivirus shRNAs against YTHDC1, YTHDC2,
768 ALKBH5, ZFC3H1 or scrambled control. Note that "ZFC3H1-2" denotes shRNA #2 against
769 ZFC3H1 as described previously (Lee et al. 2022). Lysates were collected after 96 hours,
770 separated by SDS-PAGE and immunoprobed for YTHDC1, YTHDC2, ALKBH5, ZFC3H1,
771 tubulin or mAb414, which recognizes FG-Nucleoporin proteins. To effectively deplete YTHDC1
772 and YTHDC2, cells were treated with lentivirus containing two shRNAs against YTHDC1 and
773 another two against YTHDC2.

774 (B-C) Control- or YTHDC1/2-, ALKBH5-, ZFC3H1-depleted U2OS cells were transfected with
775 the intronless *ftz* reporter plasmid (+/- 5′SS) and 5′SS motif containing reporter that lacks m6A
776 methylation sites (*no-m6A-ftz-Δi-5′SS*). 18-24 hours later the cells were fixed and the mRNA was
777 visualized by FISH. Representative images are shown in (B), scale bar = 20 µm, and
778 quantification is shown in (C). Each bar represents the average and standard error of three
779 independent experiments, each experiment consisting of at least 30 to 60 cells. Student t-test was
780 performed, * $p < 0.05$, ** $p < 0.01$, *** $p < 0.001$.

781 (D) Schematic of *PCF11-IPA* RNA reporter. The position of the FISH probe used to visualize the
782 IPA transcript is marked in gray and the position of the 3′ cleavage site in the intron is as
783 indicated.

784 (E-F) Similar to (B-C), except that Control-, YTHDC1/YTHDC2- or ALKBH5-depleted cells
785 were transfected with the *PCF11-IPA* RNA reporter.

786 (G-H) Total RNA was isolated from whole cell lysates (G) or nuclear and cytoplasmic fractions
787 (H) from control- or YTHDC1/2-, ZFC3H1-depleted U2OS cells. *PCF11* IPA was assessed by
788 qRT-PCR using oligo-dT to generate cDNA and intronic-specific primers for the amplicon.
789 Levels were normalized to the control depletion. Note that no signal was detected in reactions
790 lacking reverse transcriptase (not shown). Each bar represents the average and standard error of
791 three (G) or two (H) independent experiments.

792

793 **Figure 4. m6A methylation marks accumulate in IPA transcripts**

794 (A-B) m6A deposition was assessed by m6A-miCLIP RNA-seq from HEK293 cells. For each
795 intronic region that generates an IPA, an exon that was length (+/-10%) and expression (+/-10%)
796 matched was randomly selected. This procedure was repeated 5 times to generate 6 sets (IPAs
797 and exons Rep 1-5). The six sets were then compared for the average number and standard
798 deviation of m6A sites (A) or by stratifying them based on number of sites (B). To ensure
799 reproducibility, the relative expression of intronic regions that generate IPAs and exons were
800 determined based on two independent RNAseq experiments ("Sequencing 1" and "Sequencing
801 2").

802 (C) Meta-analysis of m6A density (as determined by m6A-miCLIP RNA-seq) along intronic
803 portions of IPA transcripts (dark blue) and all exons (cyan). The position of the 5′SS motif and
804 poly(A) site is indicated. In IPA transcripts, m6A methylation marks are enriched near the 5′SS
805 motif and poly(A) sites. In exons, m6A methylation marks are depleted from the 5′ and 3′ ends
806 (i.e. near exon-exon junctions), as documented by others.

807 (D-F) Three examples of IPA transcripts that accumulate m6A marks. IGV browser tracks are
808 shown for miCLIP density. Intronic cleavage/polyadenylation sites are indicated by the red
809 arrows. Total RNA sequencing levels in U2OS cells from previously published work (Lee et al.
810 2022) is shown. Note that the levels of IPA transcripts are upregulated following ZFC3H1-
811 depletion (shZFC).

812

813 **Figure 5. 5′SS motif containing mRNAs are transferred from nuclear speckles to YTHDC1-**
814 **containing foci in an m6A-dependent manner**

815 (A-B) Plasmid DNA containing the *ftz-Δi-5'SS* or *no-m6A-ftz-Δi-5'SS* reporter genes was
816 microinjected into U2OS nuclei. One hour post-injection, cells were fixed and stained for *ftz*
817 mRNA by FISH and SC35 by immunofluorescence. Representative cells are shown in (B), each
818 row represents a single field of view. The merged image shows mRNA in red and SC35 in green.
819 Speckles containing mRNA are indicated by arrows and the scale bar = 10μm. Individual nuclear
820 speckles (as detected by SC35) were analysed for colocalization with *ftz* mRNA by Pearson's
821 Correlation Analysis (B) as previously described (Akef et al. 2013). Each bar is the average and
822 standard error of the mean of three experiments, each experiment consist of 100 nuclear speckles
823 analysed from 10 cells.

824 (C-D) Plasmid DNA containing the *ftz-Δi-5'SS* or *no-m6A-ftz-Δi-5'SS* reporter genes was
825 transfected into U2OS. 24 hours post-transfection, cells were fixed and stained for *ftz* mRNA by
826 FISH and for YTHDC1 and SC35 by immunofluorescence. Representative cells are shown in
827 (C), each row represents a single field of view. The merged image shows mRNA in red,
828 YTHDC1 in green and SC35 in blue. *Ftz* mRNA foci are indicated by arrows and the scale bar =
829 10μm. Individual *ftz* mRNA foci were analysed for colocalization with either SC35 (y-axis) or
830 YTHDC1 (x-axis) by Pearson's Correlation Analysis (D). Each dot represents a single mRNA
831 foci (each cell containing 5-10 foci, cells were obtained from two independent experiments).

832 (E) Model of how m6A modifications are required for the nuclear surveillance of 5′SS motif
833 containing mRNAs (see text for more details).

834

835 **Supplemental Figures**

836 **Supplemental Figure 1. (Related to Figure 1)**

837 (A) Co-immunoprecipitation HEK cell lysates were treated with or without RNaseA/T1,
838 separated on a denaturing agarose gel and stained overnight with SYBR Gold. 28S and 18S
839 rRNA bands are visible in the mock treated samples but not present in the RNaseA/T1 treated
840 samples.

841 (B-C) Densitometry analysis of immunoprecipitations where the fraction of protein in the input
842 that is present precipitate is quantified (Figure 1B-D).

843 (D-F) HEK cells were transfected with FLAG-HA-YTHDC1 and lysed after 24 hours. The
844 samples were separated by SDS-PAGE and immunoblotted with antibodies against HA (which

845 detects the tagged YTHDC1), YTHDC1 (which detects the tagged and endogenous YTHDC1)
846 and ZFC3H1. (E) Quantification of tagged and untagged YTHDC1 levels using densitometry
847 analysis. Levels of each protein were normalized to tubulin and to untransfected samples. (F)
848 Quantification of endogenous ZFC3H1 levels, normalized similar to (E).

849 (G-I) Similar to (D-F), except that FLAG-ZFC3H1-HA was transfected in HEK cells.

850

851 **Supplemental Figure 2. (Related to Figure 2E-F)**

852 (A-B) U2OS cells were treated with 100 μM STM2547 or DMSO for 24 hours. Samples were
853 separated by SDS-PAGE and immunoblotted for ZFC3H1, YTHDC1, YTHDC2 and U1-70K (A)
854 which were then quantified by densitometry analysis (B) where protein levels are normalized to
855 tubulin and DMSO treated cells.

856

857 **Supplemental Figure 3. (Related to Figure 3)**

858 (A-B) Similar to Figure 3A, U2OS cells were treated with different lentivirus shRNAs against
859 YTHDC1, YTHDC2, ZFC3H1 or scrambled control (shCtrl). Lysates were collected after 96
860 hours, separated by SDS-PAGE and immunoprobed for YTHDC1, YTHDC2 and ZFC3H1 (A)
861 and then quantified by densitometry analysis (B) where protein levels are normalized to tubulin
862 and shCtrl samples.

863 (C) Schematic of *CCDC71-IPA* RNA reporter. The position of the FISH probe used to visualize
864 the IPA RNA is marked in gray and the position of the 3′ cleavage site in the intron is as
865 indicated.

866 (D-E) Control- or YTHDC1/2-, ALKBH5-, ZFC3H1-depleted U2OS cells were transfected with
867 the *CCDC71-IPA* RNA reporter, which was analysed similar to Figure 3E-F.

868 (F) U2OS cells were fractionated into nuclear and cytoplasmic fractions which were separated by
869 SDS-PAGE and immunoprobed with various protein markers to determine the purity of each
870 fraction; Lamin B1 (nucleus), tubulin (cytoplasm) and TRAP- α (endoplasmic reticulum).

871 (G) Similar to (F), except immunoprobed for ALKBH5. To determine the purity of each fraction
872 ALY (nuclear marker) and tubulin (cytoplasmic marker) were probed.

873

Lee_Fig1

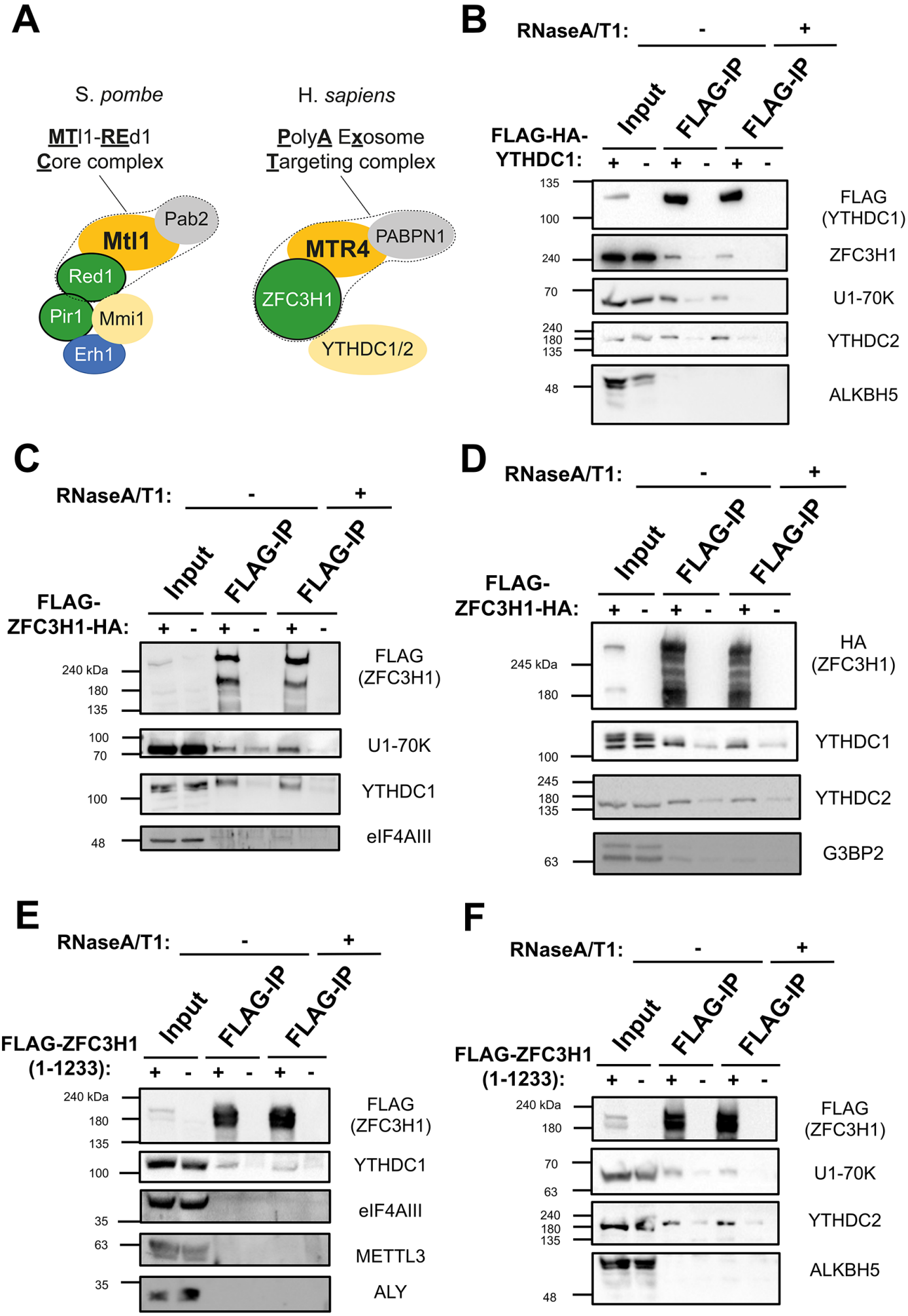
A
S. pombe
MTl1-REd1
Core complex
Mtl1
Pab2
Red1
Pir1
Mmi1
Erh1
H. sapiens
PolyA Exosome
Targeting complex
MTR4
PABPN1
ZFC3H1
YTHDC1/2
B
RNaseA/T1: - +
Input
FLAG-IP
FLAG-IP
FLAG-HA-YTHDC1: + - + - + -
135
100
240
70
240
180
135
48
FLAG (YTHDC1)
ZFC3H1
U1-70K
YTHDC2
ALKBH5
C
RNaseA/T1: - +
Input
FLAG-IP
FLAG-IP
FLAG-ZFC3H1-HA: + - + - + -
240 kDa
180
135
100
70
100
48
FLAG (ZFC3H1)
U1-70K
YTHDC1
eIF4AIII
D
RNaseA/T1: - +
Input
FLAG-IP
FLAG-IP
FLAG-ZFC3H1-HA: + - + - + -
245 kDa
180
100
245
180
135
63
HA (ZFC3H1)
YTHDC1
YTHDC2
G3BP2
E
RNaseA/T1: - +
Input
FLAG-IP
FLAG-IP
FLAG-ZFC3H1 (1-1233): + - + - + -
240 kDa
180
135
100
35
63
35
FLAG (ZFC3H1)
YTHDC1
eIF4AIII
METTL3
ALY
F
RNaseA/T1: - +
Input
FLAG-IP
FLAG-IP
FLAG-ZFC3H1 (1-1233): + - + - + -
240 kDa
180
70
63
240
180
135
48
FLAG (ZFC3H1)
U1-70K
YTHDC2
ALKBH5

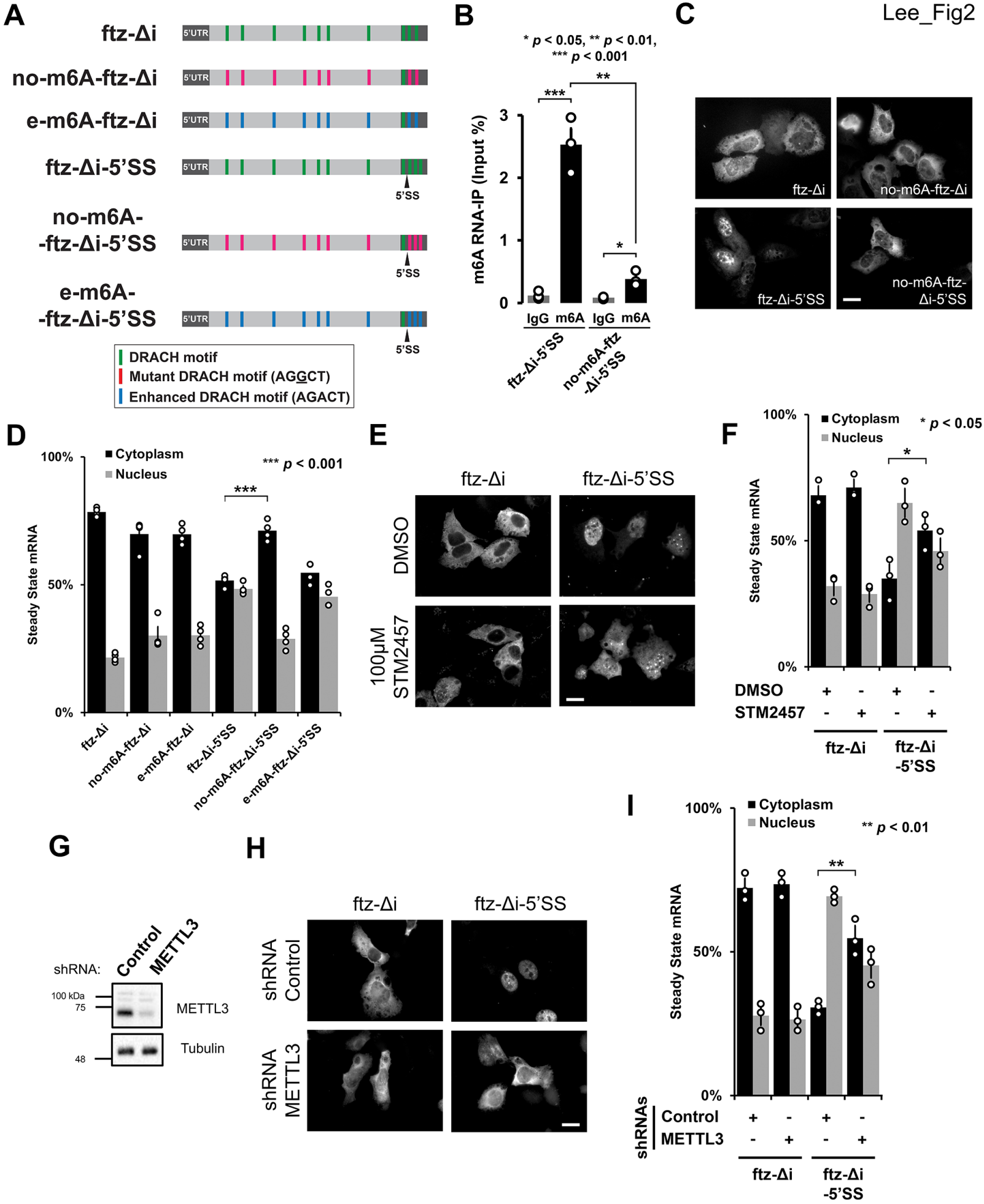
A
ftz-Δi
no-m6A-ftz-Δi
e-m6A-ftz-Δi
ftz-Δi-5'SS
no-m6A-ftz-Δi-5'SS
e-m6A-ftz-Δi-5'SS
5'UTR
5'SS
DRACH motif
Mutant DRACH motif (AGGCT)
Enhanced DRACH motif (AGACT)
B
* p < 0.05, ** p < 0.01, *** p < 0.001
m6A RNA-IP (Input %)
IgG m6A IgG m6A
ftz-Δi-5'SS
no-m6A-ftz-Δi-5'SS
C
ftz-Δi
no-m6A-ftz-Δi
ftz-Δi-5'SS
no-m6A-ftz-Δi-5'SS
D
Cytoplasm
Nucleus
*** p < 0.001
Steady State mRNA
100%
50%
0%
ftz-Δi
no-m6A-ftz-Δi
e-m6A-ftz-Δi
ftz-Δi-5'SS
no-m6A-ftz-Δi-5'SS
e-m6A-ftz-Δi-5'SS
E
ftz-Δi
ftz-Δi-5'SS
DMSO
100μM STM2457
F
Cytoplasm
Nucleus
* p < 0.05
Steady State mRNA
DMSO
STM2457
ftz-Δi
ftz-Δi -5'SS
G
shRNA:
Control
METTL3
100 kDa
75
48
METTL3
Tubulin
H
ftz-Δi
ftz-Δi-5'SS
shRNA Control
shRNA METTL3
I
Cytoplasm
Nucleus
** p < 0.01
Steady State mRNA
shRNAs
Control
METTL3
ftz-Δi
ftz-Δi -5'SS

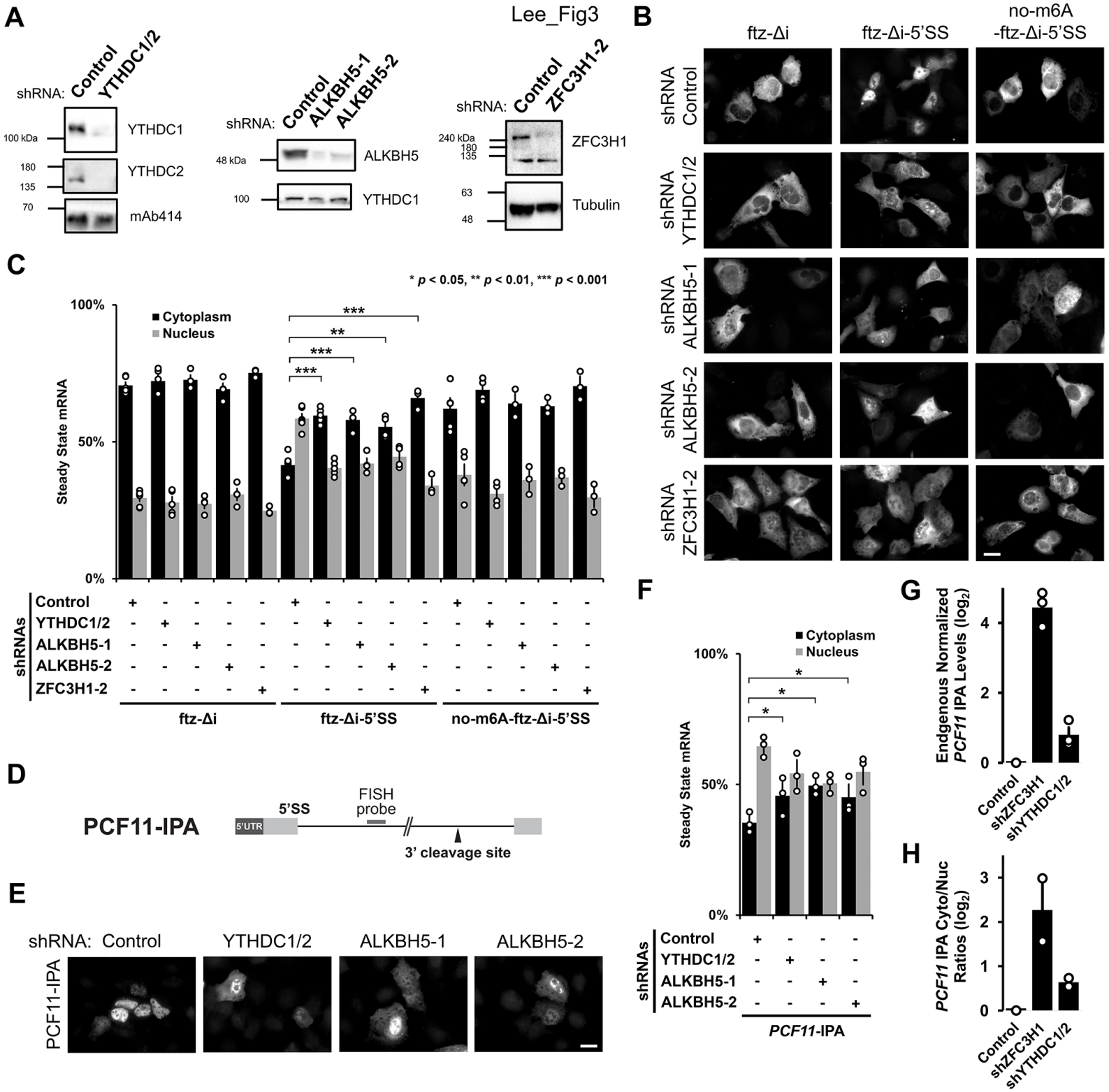
Lee_Fig3
A
shRNA: Control YTHDC1/2
100 kDa
YTHDC1
180
135
YTHDC2
70
mAb414
shRNA: Control ALKBH5-1 ALKBH5-2
48 kDa
ALKBH5
100
YTHDC1
shRNA: Control ZFC3H1-2
240 kDa
180
135
ZFC3H1
63
48
Tubulin
B
ftz-Δi
ftz-Δi-5'SS
no-m6A -ftz-Δi-5'SS
shRNA Control
shRNA YTHDC1/2
shRNA ALKBH5-1
shRNA ALKBH5-2
shRNA ZFC3H1-2
C
* p < 0.05, ** p < 0.01, *** p < 0.001
100%
50%
0%
Steady State mRNA
Cytoplasm
Nucleus
shRNAs
Control
YTHDC1/2
ALKBH5-1
ALKBH5-2
ZFC3H1-2
ftz-Δi
ftz-Δi-5'SS
no-m6A-ftz-Δi-5'SS
D
PCF11-IPA
5'UTR
5'SS
FISH probe
3' cleavage site
E
shRNA: Control
YTHDC1/2
ALKBH5-1
ALKBH5-2
PCF11-IPA
F
100%
50%
0%
Steady State mRNA
Cytoplasm
Nucleus
shRNAs
Control
YTHDC1/2
ALKBH5-1
ALKBH5-2
PCF11-IPA
G
Endgenous Normalized PCF11 IPA Levels (log2)
Control
shZFC3H1
shYTHDC1/2
H
PCF11 IPA Cyto/Nuc Ratios (log2)
Control
shZFC3H1
shYTHDC1/2

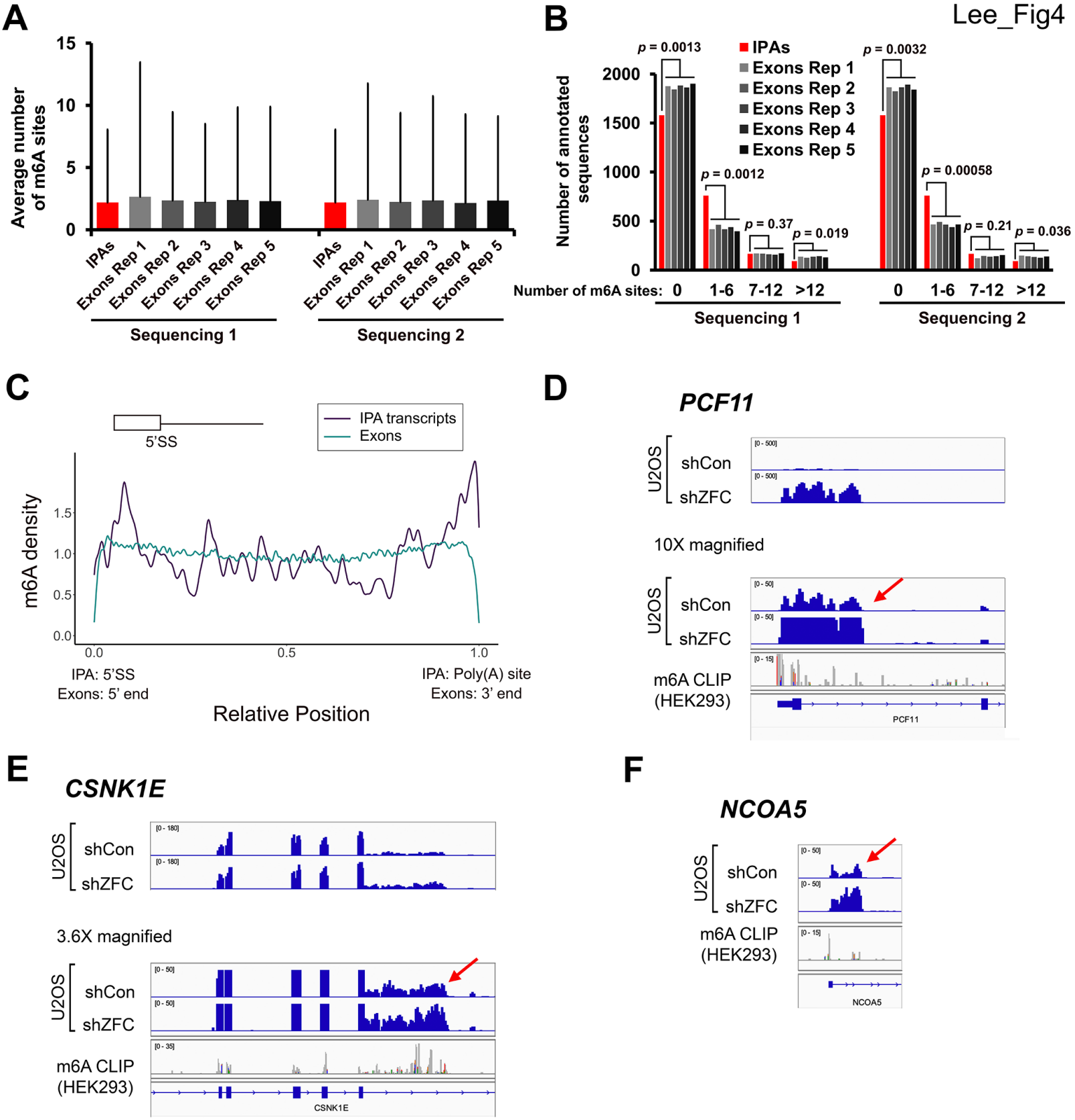
Lee_Fig4
A
Average number of m6A sites
15
10
5
0
IPAs
Exons Rep 1
Exons Rep 2
Exons Rep 3
Exons Rep 4
Exons Rep 5
Sequencing 1
Sequencing 2
B
Number of annotated sequences
2000
1500
1000
500
0
p = 0.0013
p = 0.0012
p = 0.37
p = 0.019
p = 0.0032
p = 0.00058
p = 0.21
p = 0.036
Number of m6A sites: 0 1-6 7-12 >12
C
5'SS
IPA transcripts
Exons
m6A density
1.5
1.0
0.5
0.0
IPA: 5'SS
Exons: 5' end
IPA: Poly(A) site
Exons: 3' end
Relative Position
D
PCF11
U2OS
shCon
shZFC
10X magnified
m6A CLIP (HEK293)
E
CSNK1E
3.6X magnified
F
NCOA5

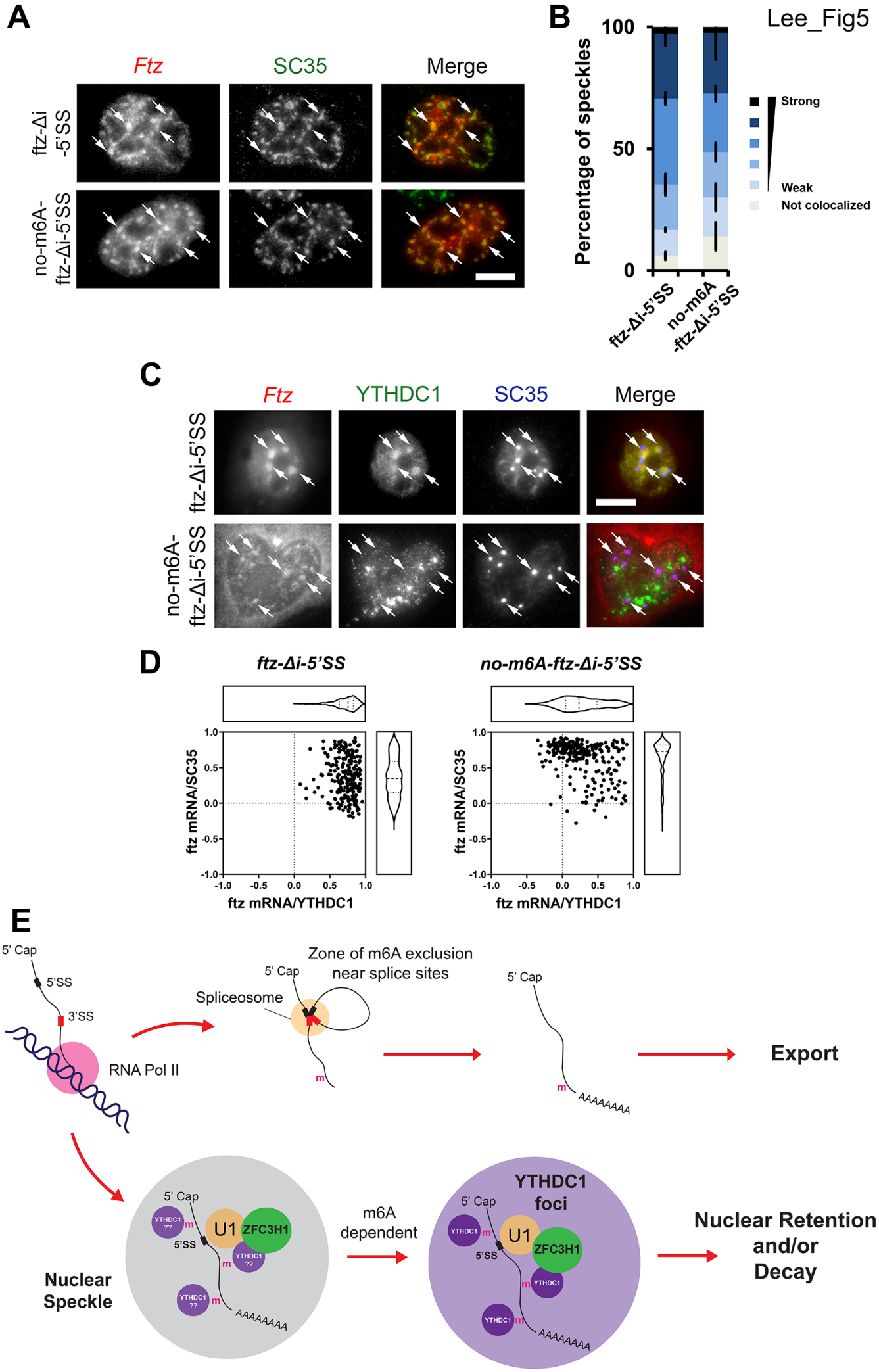
A
Ftz
SC35
Merge
ftz-Δi -5'SS
no-m6A-ftz-Δi-5'SS
B
Lee_Fig5
Percentage of speckles
100
50
0
Strong
Weak
Not colocalized
ftz-Δi-5'SS
no-m6A -ftz-Δi-5'SS
C
Ftz
YTHDC1
SC35
Merge
ftz-Δi-5'SS
no-m6A-ftz-Δi-5'SS
D
ftz-Δi-5'SS
no-m6A-ftz-Δi-5'SS
ftz mRNA/SC35
ftz mRNA/YTHDC1
1.0
0.5
0.0
-0.5
-1.0
E
5' Cap
5'SS
3'SS
RNA Pol II
Spliceosome
Zone of m6A exclusion
near splice sites
m
AAAAAAAA
Export
Nuclear Speckle
YTHDC1 ??
U1
ZFC3H1
m6A
dependent
YTHDC1 foci
YTHDC1
Nuclear Retention
and/or
Decay

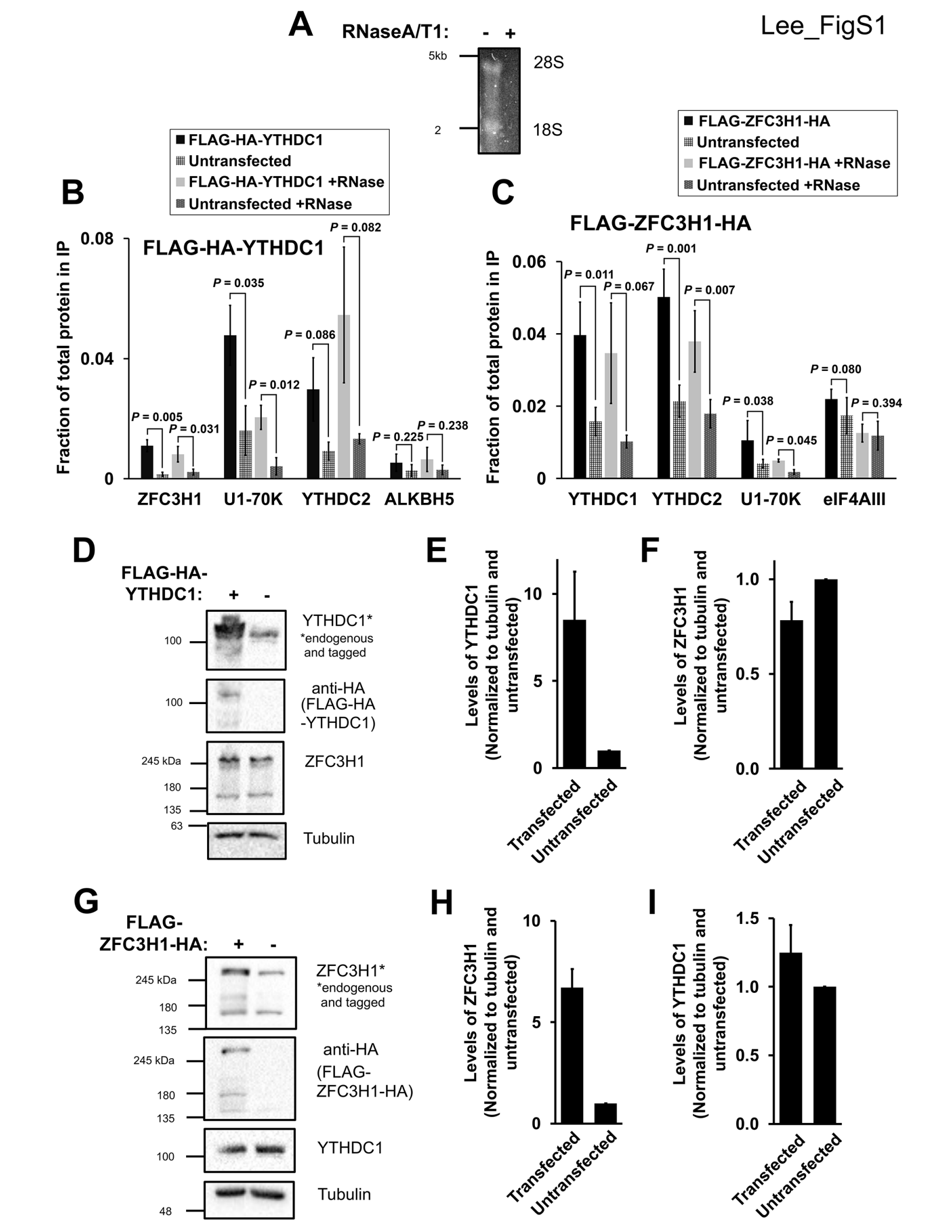
Lee_FigS1
A
RNaseA/T1: - +
5kb
2
28S
18S
B
FLAG-HA-YTHDC1
Untransfected
FLAG-HA-YTHDC1 +RNase
Untransfected +RNase
FLAG-HA-YTHDC1
Fraction of total protein in IP
0.08
0.04
0
P = 0.005
P = 0.031
P = 0.035
P = 0.012
P = 0.086
P = 0.082
P = 0.225
P = 0.238
ZFC3H1
U1-70K
YTHDC2
ALKBH5
C
FLAG-ZFC3H1-HA
Untransfected
FLAG-ZFC3H1-HA +RNase
Untransfected +RNase
FLAG-ZFC3H1-HA
Fraction of total protein in IP
0.06
0.04
0.02
0
P = 0.011
P = 0.067
P = 0.001
P = 0.007
P = 0.038
P = 0.045
P = 0.080
P = 0.394
YTHDC1
YTHDC2
U1-70K
eIF4AIII
D
FLAG-HA-YTHDC1: + -
100
YTHDC1*
*endogenous and tagged
100
anti-HA (FLAG-HA -YTHDC1)
245 kDa
180
135
63
ZFC3H1
Tubulin
E
Levels of YTHDC1 (Normalized to tubulin and untransfected)
10
5
0
Transfected
Untransfected
F
Levels of ZFC3H1 (Normalized to tubulin and untransfected)
1.0
0.5
0.0
Transfected
Untransfected
G
FLAG-ZFC3H1-HA: + -
245 kDa
180
135
ZFC3H1*
*endogenous and tagged
245 kDa
180
135
anti-HA (FLAG-ZFC3H1-HA)
100
YTHDC1
48
Tubulin
H
Levels of ZFC3H1 (Normalized to tubulin and untransfected)
10
5
0
Transfected
Untransfected
I
Levels of YTHDC1 (Normalized to tubulin and untransfected)
1.5
1.0
0.5
0.0
Transfected
Untransfected

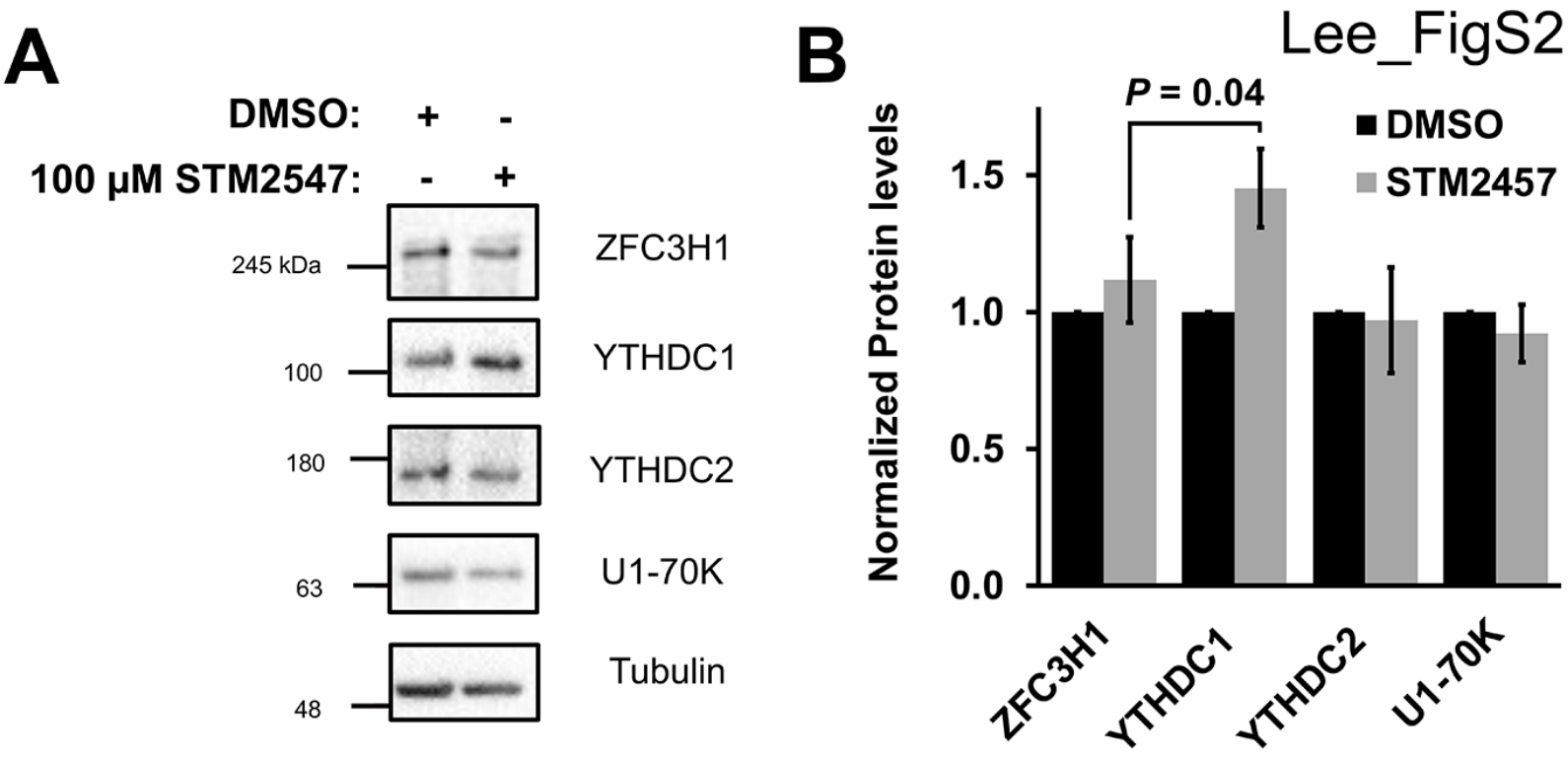
A
DMSO: + -
100 μM STM2547: - +
245 kDa
100
180
63
48
ZFC3H1
YTHDC1
YTHDC2
U1-70K
Tubulin
B
Lee_FigS2
P = 0.04
DMSO
STM2457
Normalized Protein levels
1.5
1.0
0.5
0.0
ZFC3H1
YTHDC1
YTHDC2
U1-70K

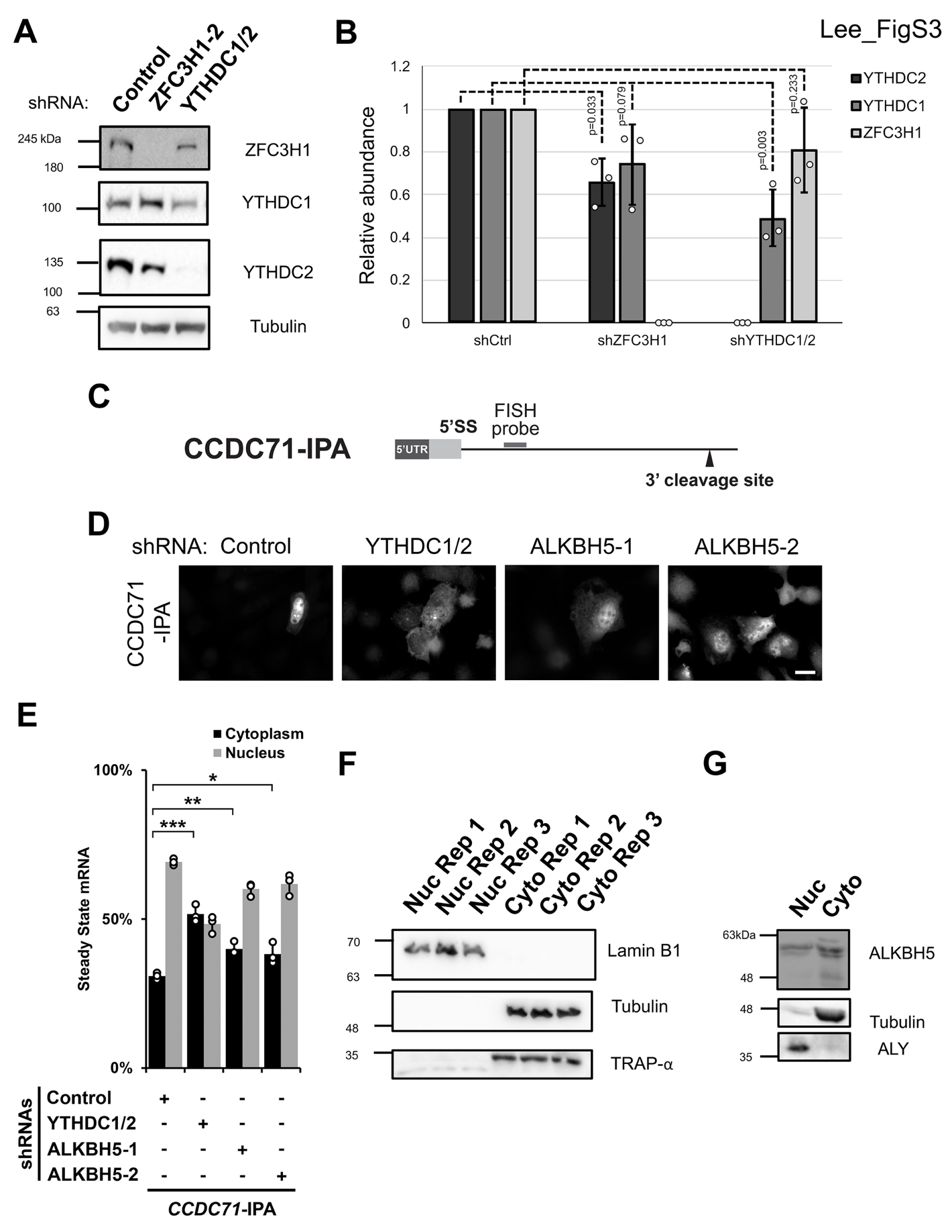
Lee_FigS3
A
shRNA:
Control
ZFC3H1-2
YTHDC1/2
245 kDa
180
100
135
100
63
ZFC3H1
YTHDC1
YTHDC2
Tubulin
B
Relative abundance
1.2
1
0.8
0.6
0.4
0.2
0
p=0.033
p=0.079
p=0.003
p=0.233
YTHDC2
YTHDC1
ZFC3H1
shCtrl
shZFC3H1
shYTHDC1/2
C
CCDC71-IPA
5'SS
FISH probe
5'UTR
3' cleavage site
D
shRNA: Control
YTHDC1/2
ALKBH5-1
ALKBH5-2
CCDC71 -IPA
E
Cytoplasm
Nucleus
100%
50%
0%
Steady State mRNA
*
**
***
shRNAs
Control + - - -
YTHDC1/2 - + - -
ALKBH5-1 - - + -
ALKBH5-2 - - - +
CCDC71-IPA
F
Nuc Rep 1
Nuc Rep 2
Nuc Rep 3
Cyto Rep 1
Cyto Rep 2
Cyto Rep 3
70
63
48
35
Lamin B1
Tubulin
TRAP-α
G
Nuc
Cyto
63kDa
48
48
35
ALKBH5
Tubulin
ALY